Dynamic Acousto-Elastic Testing

Sylvain Haupert, Guillaume Renaud, Jacques Rivière, Parisa Shokouhi

Chapter 13
Dynamic Acousto-Elastic Testing

Sylvain Haupert, Guillaume Renaud, Jacques Riviere, and Parisa Shokouhi

13.1 Introduction

13.1.1 Inspirations and Principles of Dynamic Acousto-Elastic Testing

Pioneering measurements of elastic nonlinearity were static methods leading to the thermodynamic diagram that shows the relations between pressure, volume, and temperature (p-v-T diagram) [1]. The dependence of the bulk elastic modulus on the pressure, i.e., a measure of nonlinear elasticity, was deduced from this diagram. In the beginning of the twentieth century, resonance spectroscopy [2, 3] or methods based on interferometry [4] were proposed to measure the elastic moduli as functions of temperature and hydrostatic pressure. Finally, with the possibility of generating an ultrasonic short pulse [5, 6], acousto-elastic testing became an alternative way to assess elastic nonlinearity. Acousto-elastic testing consists in measuring changes of the speed of sound (by the determination of the travel time of an ultrasonic short pulse) induced by a hydrostatic or uniaxial stress (or strain). For metals and polymers, the relative variation in ultrasound wave-speed is found

S. Haupert · G. Renaud (✉)
Sorbonne Universités, UPMC, CNRS, INSERM, Laboratoire d'Imagerie Biomédicale, Paris, France
e-mail: guillaume.renaud@upmc.fr

J. Riviere
Institut des Sciences de la Terre (ISTerre), CNRS, Grenoble, France

Department of Geosciences, Penn State University, State College, PA, USA

P. Shokouhi
Department of Civil and Environmental Engineering, Penn State University, State College, PA, USA

T. Kundu (ed.), *Nonlinear Ultrasonic and Vibro-Acoustical Techniques for Nondestructive Evaluation*, https://doi.org/10.1007/978-3-319-94476-0_13

between 10^{-5} and 10^{-4} per MPa of the applied stress. In cracked or granular media, contacts between the two lips of cracks or contacts between grains can greatly increase the variation in ultrasound wave-speed up to about 10^{-2} per MPa of applied stress, i.e., orders of magnitude larger than in metals and polymers [7].

A conventional acousto-elastic experiment is quasi-static; the applied stress is varied in discrete steps and the ultrasonic wave-speed is measured for each level of the applied stress [8–10]. While early conventional experiments applied a static stress up to 1 GPa [6, 11], recent studies have applied less than 10 MPa [12]. There exist several ways to monitor the change of wave-speed induced by the quasi-static loading. It can rely on an elastic wave (propagating short ultrasonic burst or resonance technique) or on a hybrid optical and ultrasonic approach using diffraction of light by standing elastic wave [13] or Brillouin spectroscopy [14].

In the past three decades, alternative ways to measure the acousto-elastic effect were proposed. A slowly varying sinusoidal loading was proposed instead of a quasi-static stress that is varied in discrete steps [15]. Methods based on the interaction of two bulk elastic waves [16] or surface waves [17, 18] were introduced, including a technique termed Dynamic Acousto-Elastic Testing (DAET) [19, 20]. DAET is the dynamic analog of a conventional experiment of acousto-elasticity, though with significant differences. Firstly, the applied stress is not produced by a universal testing machine in discrete steps but induced by an elastic wave. The elastic wave has typically a frequency of a few kHz in a lab experiment. Consequently the elastic constants at stake are all adiabatic elastic constants. On the contrary both adiabatic and isothermal elastic constants are involved in a quasi-static conventional acousto-elastic experiment (since a quasi-static deformation is considered to be an isothermal process). Secondly, a low vibrational strain is applied, typically 10^{-6}, while conventional quasi-static experiments operate with an applied strain exceeding 10^{-4}. Finally DAET explores the dynamic elastic behavior of a material about its equilibrium state. Unlike conventional quasi-static experiments where a compressive stress only (or tensile stress only) is applied, both tensile and compressive behaviors are investigated in DAET.

In a typical DAET lab experiment, the sample is dynamically excited by an acoustic/elastic wave whose wavelength is larger than the size of the sample (frequency is typically a few kHz if the sample size is several centimeters). This wave is called the “pump” wave. A sequence of identical ultrasonic short bursts (with a typical center frequency of 1 MHz) is simultaneously applied to measure the dynamic change of elasticity induced by this pump wave. The ultrasonic short bursts are called the “probe” wave, since they are broadcasted to capture the dynamic variation in material elasticity induced by the pump wave (see Fig. 13.1). The repetition rate of these ultrasonic short bursts is chosen to adequately sample the changes of elasticity produced at a rate imposed by the temporal frequency of the pump wave. Typically the pump wave produces a dynamic acoustic displacement of the order of 1 micrometer while the ultrasonic probe induces a dynamic acoustic displacement of the order of 1 nm. Therefore, the theory of acousto-elasticity as described in [7] can be applied to DAET.

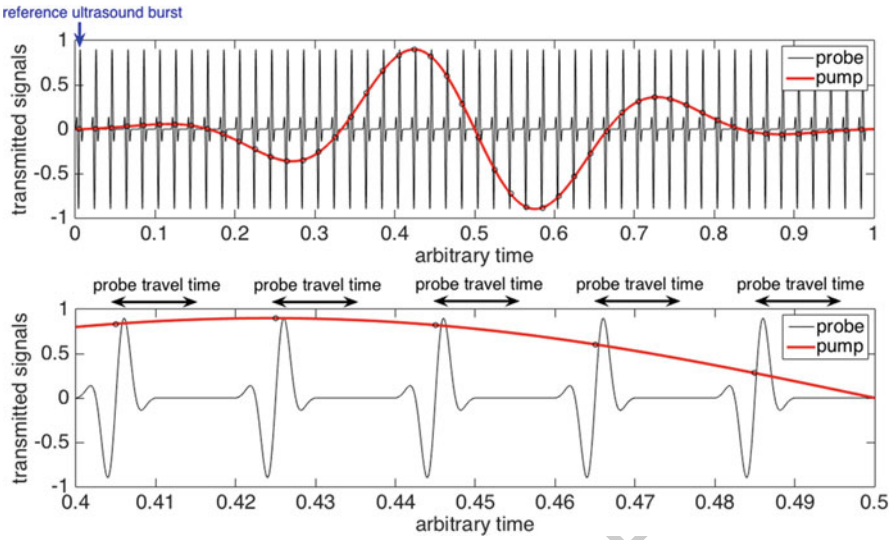

AQ3

Fig. 13.1 Principles of DAET. Top: schematic representation of the pump wave and the probe wave. The very first ultrasonic pulse is used as a reference. Bottom: enlargement showing that the travel time of an ultrasonic pulse is much smaller than the temporal period of the pump wave

In order to apply the theory of acousto-elasticity [7], the strain field (produced by the pump wave) traversed by the ultrasonic pulses must be quasi-homogeneous and quasi-static with respect to the ultrasonic travel time in the sample. The geometry of the sample and/or the position of the ultrasound transducers that transmit and receive the ultrasonic pulses are then selected so that the travel time of the probe wave (ultrasonic pulses) is much smaller than the temporal period of the pump wave. Each ultrasonic pulse traverses the material as it experiences a different strain level and the large number of ultrasonic pulses in the sequence (typically 1000–10,000). This provides a dense sampling of the relation between the ultrasonic wave-speed measured by the probe wave and the applied strain (produced by the pump wave). The change of ultrasonic wave-speed is calculated from the change of travel time of the probe wave, since the length of the propagation path is known. The change of travel time can be precisely determined from a comparison of a given ultrasonic pulse in the sequence with the very first ultrasonic pulse that serves as a reference (see Fig. 13.1). Techniques to achieve this will be detailed later in this chapter. For each ultrasonic pulse, the strain level is taken as the spatial and temporal average of the strain experienced by the ultrasonic pulse during its propagation through the sample. Techniques to calculate the strain value associated with each ultrasonic pulse will also be explained later in this chapter.

13.1.2 Comparison with Other Methods

DAET belongs to the family of "pump-probe" methods that have existed in nonlinear acoustics from the 1950s [21, 22]. It involves two dynamic fields: one perturbs the material elasticity (the pump) and one measures the induced elastic changes (the probe). Experiments of this type are also termed nonlinear wave mixing. In such measurements, one is interested in the resulting effects of the nonlinear interaction after a propagation distance (i.e., length of interaction) that is much larger than both the pump wavelength and the probe wavelength (see Chaps. 1 and 6 in this book). In contrast, in DAET, we are interested in the nonlinear interaction between the pump wave and the probe wave over a distance that is much smaller than the pump wavelength. This situation is therefore more similar to a conventional quasi-static acousto-elastic experiment than an experiment of nonlinear wave mixing.

Nonlinear resonance ultrasound spectroscopy (NRUS, see Chaps. 2 and 12 in this book) measures a variation in the material elasticity (as the driving amplitude is increased) that is time-averaged over an acoustic period. In contrast DAET allows one to "read" the instantaneous variations in the elastic modulus during an entire acoustic cycle of the pump wave. In this respect, DAET provides more detailed insight into the dynamic elastic nonlinearity of a material than NRUS. Moreover nonlinear resonance ultrasound spectroscopy measures the global elastic nonlinearity of the entire sample. In contrast DAET provides a local measurement of elastic nonlinearity. The investigated region of the sample is the volume of the sample that is traversed by the ultrasonic short bursts (probe wave).

13.2 Experimental Setups

Dynamic acousto-elastic testing (DAET) was originally developed to evaluate microdamage in trabecular (spongious) bone [19, 23]. In this first configuration, the bone sample was immersed in a water tank. It was later shown that small modifications of this experimental setup allow one to investigate any material immersed in a coupling fluid, such as a plain block of a given solid material, water-saturated glass beads [24], gels or creams [25], or a suspension of particles [25, 26]. Meanwhile, DAET method was also extended to experimentations in contact (without the need of immersing the sample in a water tank) to study materials such as rocks [27, 28], concrete [29, 30], or metals with cracks [31, 32] under room-dry conditions.

13.2.1 Low-Frequency Pump Wave: Quasi-Homogeneous and Quasi-Static Requirements

Whether DAET is done in immersion or in contact, both setups are similar and consist in broadcasting a low-frequency (LF) pump wave and measuring changes of wave-speed experienced by an ultrasonic (US) probe wave that traverses the LF pressure/strain field generated in the probed volume. The analysis of the measurements is straightforward if two requirements are respected: the LF pressure field must be (1) quasi-homogeneous in the volume probed by the US probe wave and (2) quasi-static with regard to the travel time of the US probe wave. In these conditions, it is analogous to conventional quasi-static acousto-elastic testing.

It has been shown experimentally and validated by simulation [33] that the pressure/strain field seen by the US probe is quasi-homogeneous when the distance d_{probe} traveled by the US probe is at least 10 times smaller than the LF pump wavelength λ_{pump}, while the quasi-static requirement is reached when the US time of flight (TOF) propagation is at least 10 times smaller than the LF pump period T_{pump}. The two requirements are related via the wave-speed c since $d_{probe} = c^*TOF$ and $\lambda_{pump} = c^*T_{pump}$. In practice, the LF pump wave is either a standing wave (e.g., first compressional mode of a bar) [27, 34] or a propagative wave [20, 26, 35] (Fig. 13.2). Both configurations will be explained in detail in Sects. 13.2.4 and 13.2.5.

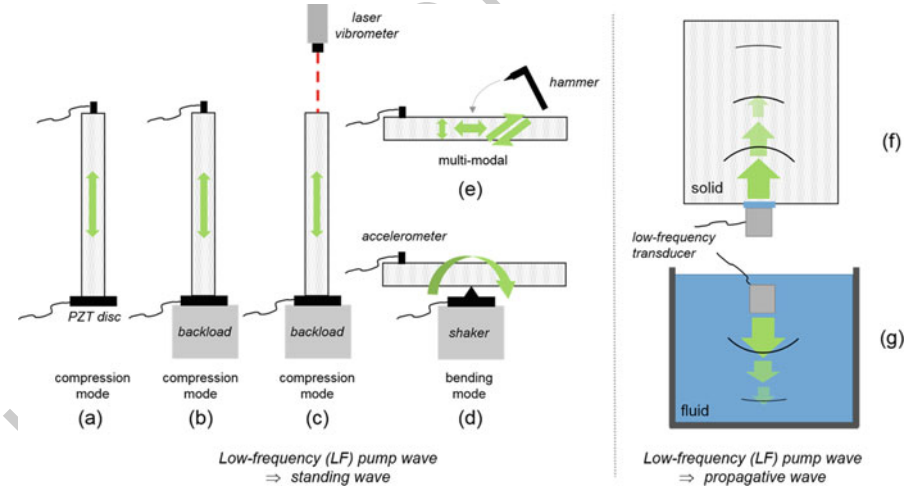

Fig. 13.2 Examples of different low-frequency (LF) pump wave configurations. For bars or cylinders, the LF pump wave can be a standing wave matching either the 1st compressional mode (**a**–**c**) or the 1st bending mode (**d**). The LF pump can also be multi-modal when using a hammer as exciter (**e**). Various boundary conditions and emitter/receiver types can be used depending on the application. For a (semi-)infinite solid (**f**) or fluid (**g**) sample, the pump can be a propagative wave induced by a LF transducer

13.2.2 *Ultrasonic Probe Wave: Type, Amplitude, Position, and Orientation*

A US probe wave is required to read the instantaneous change of phase velocity at different strain levels. While it is possible to use any kind of ultrasonic waves, bulk compressional wave is involved in most of the studies, while bulk shear wave [29, 36], or surface wave such as direct or head wave [27, 37], or Raleigh wave [29, 30] remain anecdotic. The only requirement is to be able to measure the TOF of the probe wave and its variation (induced by the pump wave, see Sect. 13.3) along a known propagation path for different strain levels. The propagation path of the probe wave is also needed to evaluate the pump strain experienced by the probe wave.

In practice, this can be done with two US transducers in direct or indirect transmission configuration or with one transducer in pulse-echo configuration (Fig. 13.3). The choice of configuration depends on the experimental conditions such as the workable surface of the sample, the material access, the attenuation in the material, or the orientation between the US probe beam and the LF pump wave (e.g., collinear, orthogonal, or with an arbitrary angle). It also depends on how large the TOF variation is along the propagation distance in the medium. If the one way direct transmission path is not enough to accumulate sufficient change in TOF (i.e., larger than the phase noise level), the use of multiple reflections (within the sample) along the same direct transmission path represents a good alternative [32].

In order to determine the propagation path of the US probe wave, a short US pulse is generally preferred as it is relatively easy to guess the propagation knowing the nature of the wave (e.g., compression or shear bulk wave, Rayleigh wave or Lamb

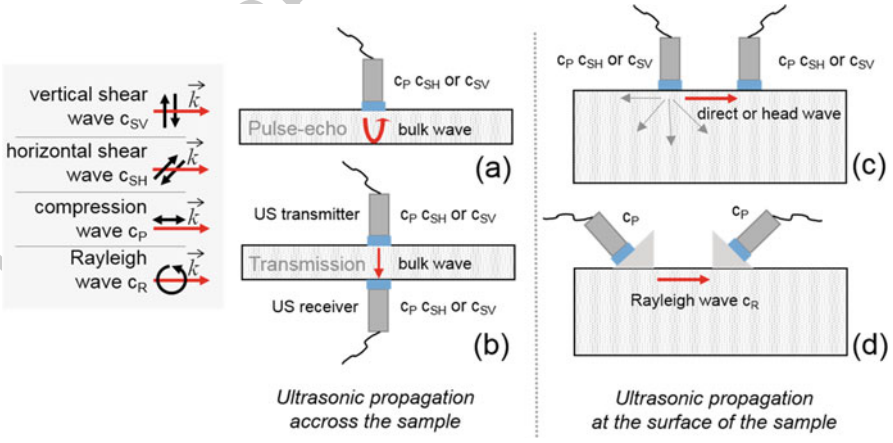

Fig. 13.3 Examples of different high-frequency (HF) probe wave configurations: bulk compression wave or bulk shear wave propagating across the sample in pulse-echo (**a**) or transmission (**b**); direct wave (**c**) or surface wave (**d**) propagating at the surface of the sample

wave). The use of a continuous monochromatic US wave may be used cautiously as waves may travel in the whole material, with possible multiple reflections and modes conversion. The probe signal recorded at the receiver contains the direct propagation signal superimposed with signals produced by reflections and mode conversion within the sample, which makes the analysis difficult. It is preferable to use a continuous probe in case of strong attenuation (e.g., due to multiple scattering and/or absorption) that reduces the amplitude of waves reflected at the sample boundaries [38].

For very heterogeneous media such as rocks or concrete, the direct or ballistic US wave is sometimes difficult to disentangle from the later arriving waves, the so-called coda. The coda is the result of multiple scattering that occurs when the US wavelength is close to the size of the scatterers and/or when the scattering efficiency is high (large contrast of mass density and/or compressibility). A coda-based technique called Coda Wave Interferometry (CWI) can be used to calculate small variations in wave-speed with a greater accuracy than ballistic wave arrival times, making it an interesting tool for measuring acousto-elastic effects [39, 40]. The main drawbacks of using coda wave instead of direct wave are (1) the LF strain field seen by the coda wave is no more quasi-homogeneous nor quasi-static and (2) the coda wave is a superposition of multiple shear and bulk waves having different speed of sound and polarization.

In the case of a porous medium like rocks, it is important to add treatment on the surface of the sample (e.g., polished nail or tape) to prevent coupling ultrasound gel from penetrating the material.

When a short US pulse is used, the pulse repetition frequency (PRF) is conditioned by the distance between the US emitter and receiver and by ultrasound attenuation. Indeed, for proper analysis, two successive US signals (including direct propagation, (multiple) reflections, guided propagation, and (multiple) scattering) must not overlap in the time domain. The ratio between the PRF and the frequency of the LF pump wave must not equal a rational number in order to create a stroboscopic effect, so that US pulses probe different LF strains during each LF cycle. In this manner, US pulses are able to probe discrete values well distributed over the entire LF strain excursion, both in tension and in compression, after several LF periods (e.g., generally between few tens to few hundreds).

13.2.3 Clock Synchronization and Phase Noise

The DAET measurement protocol involves three distinct phases (Figs. 13.1 and 13.14):

- *Pre-pump reference phase*—The US probe is turned on, and stays on until the end of the DAET measurement. During this phase, the reference TOF is measured while the noise floor (e.g., phase noise) is evaluated by computing the phase-shift between US signals (i.e., US pulses or US monochromatic continuous wave).

- *Pump phase*—The LF pump wave is then turned on. It can be an impact or continuous monochromatic wave, which lasts as long as it is needed for the US signal to probe the entire LF strain excursion. In case of standing wave, it is important to wait for the steady state. The TOF variation is evaluated by assessing the phase-shift between the instantaneous US signal and the reference US signal (see Sect. 13.3)
- *Post-pump reference phase or recovery phase*—The LF pump wave is finally turned off. In some cases, the phase velocity of the material does not return back instantaneously to its initial value, leading to a relaxation period, due to the so-called conditioning (see Sect. 13.4.2.3) that is tracked by the US probe.

The key for effective DAET measurements is to achieve high sensitivity to small TOF variations. For weakly nonlinear elastic materials, such as PMMA or duralumin, the maximum TOF variation is close to one nanosecond for a US wave traveling through a few centimeters if the maximum LF strain level is in the order of 10^{-5} [27, 41]. Although not straightforward, it is possible to achieve phase noise as low as 0.1 ns with conventional electronic devices (e.g., function generator, digitizer) if some essential rules are respected.

The most important rule is to maximize the signal-to-noise ratio of the recorded probe signal. Another important aspect is synchronization. All the electronic devices involved in the experimental setup must be synchronized by choosing a single master clock across all devices. This is generally done by connecting the 10 MHz reference clock from one of the devices (e.g., a function generator) to other electronic devices (e.g., the other function generators and digitizers). A good synchronization reduces drastically the electronic time deviation or phase-shift, also called jitter, which is one of the major sources of phase noise.

Phase noise can also be caused by relative movements of both US transducers due to low vibrations coming from the environment (e.g., vibration from the building). The use of the same holder for both US transducers overcomes this problem by suppressing the relative movements.

A good configuration for the digitizer (i.e., sampling frequency and quantization bits) is also required to achieve high sensitivity to small TOF variation. High sampling frequency is a necessity, but it does not determine directly the TOF resolution. Indeed, TOF resolution depends on the sampling frequency (i.e., sampling period) as well as the numerical tool used to compute the phase-shift between two probe signals (see Sect. 13.3).

The quantization bits (i.e., the number of vertical bits used for analog-to-digital conversion) are generally forgotten but this factor is as important as the sampling frequency. Indeed, the higher the number of quantization bits, the better will be the TOF resolution. The vertical range (i.e., in voltage) of the digitizer must also be adapted to the voltage of the US transmitted signal in order to reach at least 80% of the full range.

In practice, for short US pulses centered at around 2 MHz, a sampling frequency above 50 MHz (i.e., a sampling period of 20 ns) with a quantization above 14 bits reduces the phase noise below 0.1 ns.

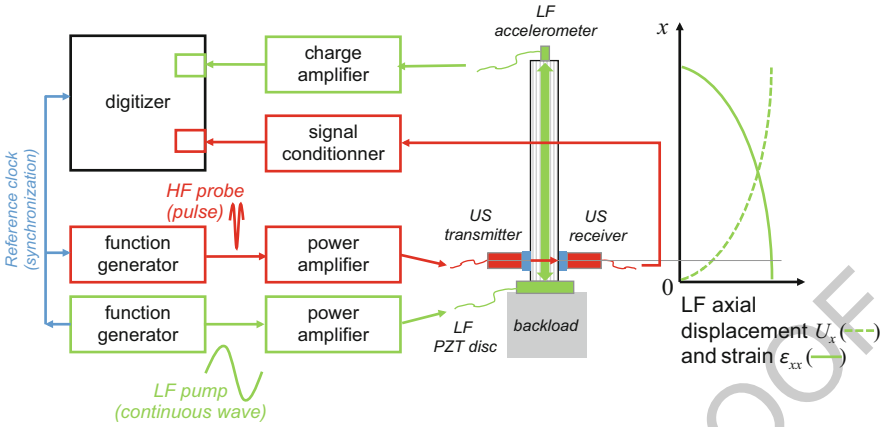

Fig. 13.4 Example of a DAET experimental setup with stationary wave (1st compression mode) as pump wave. The shape of the sample is either a bar or a cylinder

13.2.4 DAET with Stationary Pump Wave 243

DAET with stationary pump wave is recommended for laboratory measurements on calibrated samples such as bars, cylinders, or plates because it is possible: 244 245

(1) To achieve high strain level, up to 10^{-4}. 246
(2) To estimate the strain level along the US probe path as the strain distribution is known for a simple modal shape. 247 248

In practice, the first compressional [27] or flexural [30] mode is preferentially excited with a continuous monochromatic source tuned to match the frequency of the desired mode. The LF pump wave is broadcasted directly in the sample by means of a piezoelectric disk glued on the sample [27] or a shaker attached to the sample [30]. The frequency of the pump wave is chosen to match the fixed-free [27] or the free-free [42] boundary conditions (Fig. 13.2). 249 250 251 252 253 254

When using the first compressional mode with fixed-free boundary conditions, the most common configuration for the probe consists of two US transducers in through-transmission configuration, with a direction of propagation either normal to the pump stress direction (Fig. 13.4) [43], collinear to the pump stress direction [27], or at an angle [41]. The pair of US transducers is generally placed where the LF strain amplitude is the largest, i.e., close to the piezoelectric disk (Fig. 13.4). 255 256 257 258 259 260

Use of the first bending mode is more restrictive because the strain field across the sample is not uniformed. Nonetheless, along a short portion of the sample, the strain field can be considered quasi-uniform when the penetration depth (i.e., one wavelength) of the US beam is smaller than one tenth of the sample thickness. For this reason, only HF surface waves such as Rayleigh wave [30] or head wave may be used. In this configuration, the US probe is primarily sensitive to the strain component parallel to the US wave propagation direction. 261 262 263 264 265 266 267

For in situ measurements, when it is not possible/practical to glue or attach a LF source on the structure, a solution is the use of impact source, such as hammer (Fig. 13.2e). Indeed, impacting briefly the surface of the structure may select the resonant modes with the most excitability. The quick change of elasticity following the impact is either probed with short US bursts [29] or a continuous monochromatic US wave [38]. The main drawback is the difficulty to characterize the strain field seen by the US probe as multiple resonance modes are simultaneously excited.

Finally, the measurement of the in-plane or out-of-plane vibration of the sample is performed by either an accelerometer [27] or a laser vibrometer [34] (Fig. 13.2a–d). The strain is then derived directly from the particle's displacement/velocity/acceleration by analytical derivation [27]. Sometimes, when the boundary conditions are more complex, a numerical simulation is performed to compute the strain based on the experimentally measured out-of-plane or in-plane particle's displacement/velocity/acceleration [44].

13.2.5 DAET with Propagative Pump Wave

In case of in situ measurements (e.g., in soil, large concrete structures or water tank), propagating pump wave is generally the only option as no standing wave is feasible. DAET with propagative pump wave consists of a LF pressure wave that is broadcasted in an infinite medium, i.e., reflections at the boundaries of the medium are negligible (Fig. 13.5). DAET investigates the volume corresponding to the volume of interaction of the two acoustic beams (the probe beam and the pump beam).

When the infinite medium is a fluid, e.g., water, the LF pump wave can be generated by a circular piston attached to a shaker [19] or by a LF immersion transducer [26]. The LF hydrostatic pressure is measured with a hydrophone placed close to the probed volume, in order to evaluate the local pressure. Very different materials could be positioned at the volume of interaction, including solids (e.g., trabecular bone, beads), another fluid (e.g., gel or cream), or micro-particles (e.g., ultrasonic contrast agent).

When the infinite medium is a solid, e.g., soil, rock, or large concrete structure, the LF pump wave is generated at the accessible surface of the structure. In case of measurements in soil, the LF source can be the common LF source for underground prospection, such as a mobile hydraulic shaker [45]. The LF strain is deduced from two accelerometers buried in the soil at different depths [45]. These accelerometers are also used to measure the probe wave.

If one wants to reproduce propagation of seismic waves in the laboratory, a LF shear or compressional wave can be propagated in a rock [35, 46] while the LF velocity is measured by a laser vibrometer at the surface of the volume of interaction.

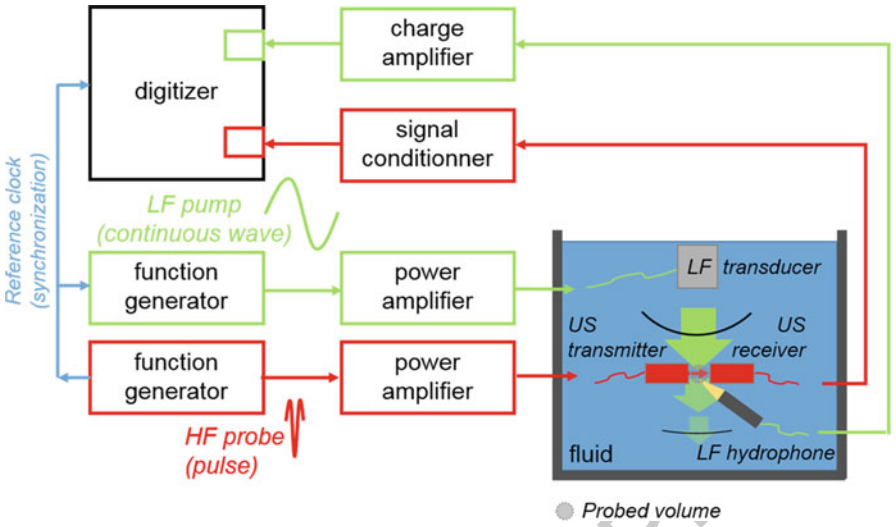

Fig. 13.5 Example of a DAET experimental setup with propagative wave as pump wave. The probed volume corresponds to the volume of interaction of the US beam and the LF beam. The medium is either a fluid or a solid

13.3 Signal Analysis

13.3.1 Analysis of the Pump: Calculation of Strain/Stress Produced by the Pump Wave That is Experienced by the Probe Wave

Most often, it is desired to know the absolute amplitude of the stress or strain generated by the pump wave. If known, it is possible to compare the elastic nonlinearity of different materials or to measure the third-order elastic constants of a material. Nonetheless, if the objective is to monitor relative changes in elastic nonlinearity of a sample over time (for instance, as a consequence of mechanical or thermal fatigue), the absolute amplitude of the pump wave is not required. In this case a non-calibrated transducer can be used to record the pump wave.

In general it is best to record the pump wave as close as possible to the path of the probe wave in the sample. In a water-borne DAET experiment, the pump wave is measured with a hydrophone, next to the sample immersed in a water tank (Fig. 13.5). In a dry DAET experiment, the pump wave is measured either with an accelerometer or with a laser interferometer or laser Doppler vibrometer (Fig. 13.2). However, the recording of the pump wave is often conducted at a position next to the path followed by the probe wave. If the absolute amplitude of the stress or strain generated by the pump wave is required, we need to determine the absolute amplitude of the pump wave experienced by the probe wave along its

path in the sample. Consequently it is necessary to take into account the differences of amplitude and phase between the recording position of the pump wave and the region traversed by the probe wave. To correct these discrepancies, it is usually necessary to measure or calculate the strain/stress field produced by the pump wave.

Moreover, the strain field produced by the pump wave is not perfectly uniform. Therefore, the strain/stress level experienced by the probe wave is taken to be the spatial average of the actual strain/stress field produced by the pump wave. Finally, even if the travel time of the probe wave is much smaller than the temporal period of the pump wave, there exists a slight temporal change of the pump amplitude during the travel time of the probe wave. Thus, for an accurate determination of the absolute amplitude of the pump wave, the strain/stress level experienced by the probe wave is taken to be the spatial and temporal average of the pump wave over the region traversed by the probe and during its travel time, respectively.

13.3.2 Analysis of the Probe: Determination of the Change of Travel Time of the Probe Wave

The objective of an experiment of acousto-elasticity is to measure the stress-dependence of the speed of sound. Since the distance of the propagation of the probe wave in the sample is known, one must determine the change of travel time of the probe wave induced by the pump wave. There are two ways to determine the change of travel time:

1. The cross-correlation method
2. The phase analysis in the frequency domain

The cross-correlation method consists in computing the cross-correlation function between a reference probe signal (the very first ultrasonic pulse of the sequence) and a second signal that is assumed to be the same waveform as the reference signal with a certain time lag. The time lag, i.e., the change of travel time, is determined by searching the time position of the maximum of the cross-correlation function (Fig. 13.6). It can be positive or negative. Any difference in the waveform that is not a simple difference of amplitude may cause a bias in the determination of the change of travel time. Furthermore a parabolic interpolation around the maximum of the cross-correlation function provides sub-sample estimation of the time delay (i.e., the change of travel time). This technique is widely used in medical ultrasound and is known to be very robust against noise [47]. With an excellent signal-to-noise ratio and an ultrasound frequency of 1 MHz, this technique is able to determine a time delay smaller than 0.1 ns.

Another way to determine a change of travel time is the phase analysis in the Fourier domain. At a given frequency f (within the frequency bandwidth of the probe wave), a phase lag $\Delta\varphi$ is simply related to a time lag Δt by $\Delta\varphi = 2\pi f \Delta t$. After computing the Fourier transform of the reference probe signal (the very first

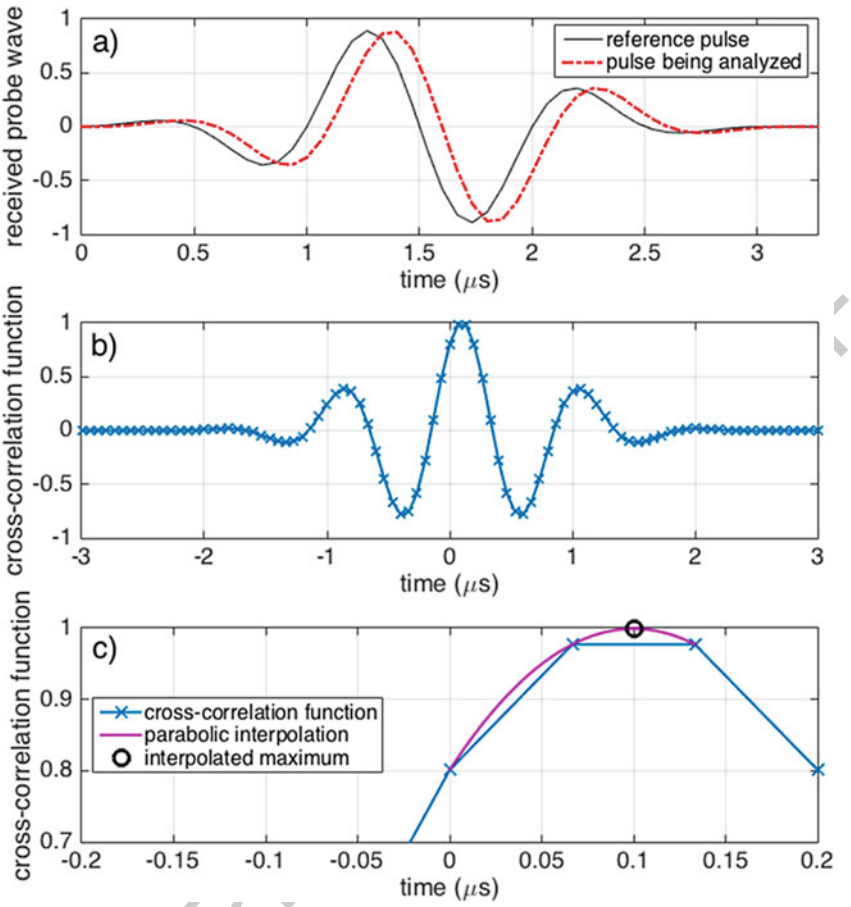

Fig. 13.6 Illustration of the cross-correlation method with synthetic signals. The ultrasonic pulse (probe wave) has a center frequency of 1 MHz and the sampling frequency is 25 MHz. (**a**) Recorded reference signal and signal to be analyzed, a time lag of 0.1 μs was introduced. (**b**) Cross-correlation function. (**c**) Enlargement of panel (**b**) showing the sub-sample determination of the time lag using a parabolic interpolation of the maximum of the cross-correlation function

ultrasonic pulse of the sequence) and the Fourier transform of one of the following ultrasonic pulses, the phase of the ratio of the two Fourier transforms gives the phase lag (Fig. 13.7). The time lag is then readily deduced. This method is less robust against noise than the cross-correlation technique, but it does not require that the two signals are identical in shape. Besides the phase method is sometimes necessary in a material where ultrasonic attenuation is significantly modified by the pump wave (see later in this chapter).

Once the change of travel time of the probe (dt) is accurately determined, the change of wave-speed of the probe (dc) can be calculated after evaluating the change in propagation distance of the probe (dL) induced by the pump strain:

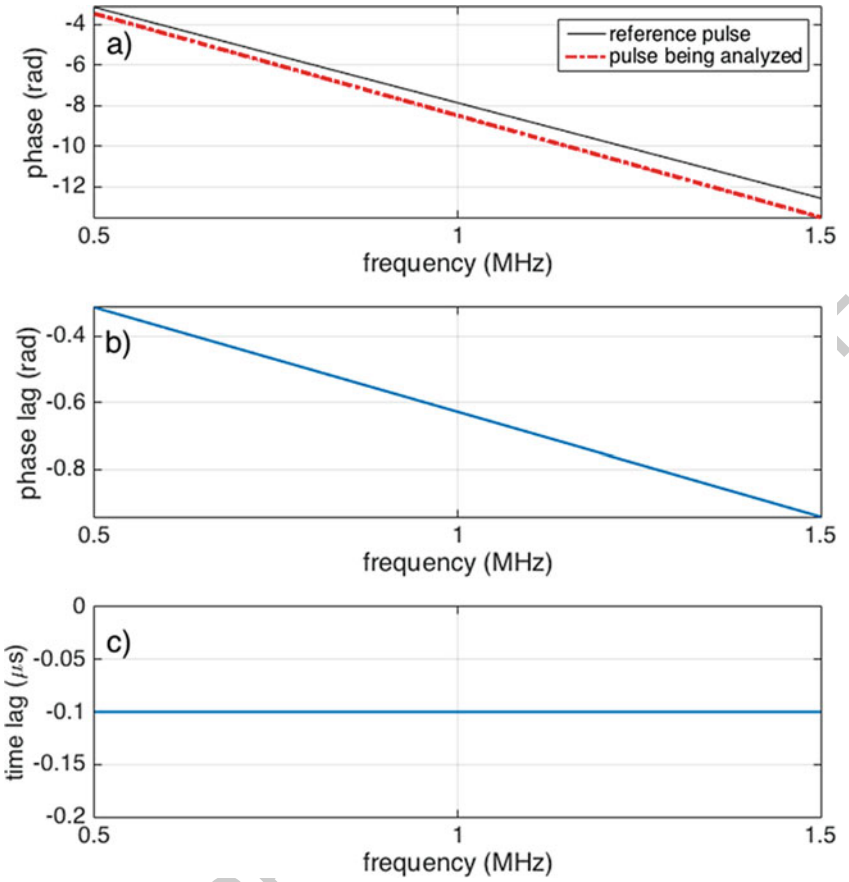

Fig. 13.7 Illustration of the phase method with the same synthetic signals as in Fig. 13.6. (**a**) Unwrapped phase of the two ultrasonic pulses. (**b**) Phase lag between the two signals. (**c**) Calculated time lag

$$\frac{dc}{c_0} = \frac{dL}{L_0} - \frac{dt}{t_0}$$

The subscript 0 refers to the value at zero pump strain (at equilibrium, in the absence of pump wave).

If the ultrasonic transducers employed to broadcast the probe and record it are attached to the sample, then dL is readily estimated knowing L_0 and the strain field produced by the pump wave.

If the ultrasonic transducers are coupled to the sample with water or gel, then the distance between the two transducers is fixed (not affected by the pump). And the formula above must be refined to take into account the variation in travel time in the coupling layer since the thickness of this coupling layer is dynamically modulated by the pump wave.

Note also that in materials with high elastic nonlinearity like granular media (rocks, concrete) the correction of the change of distance of propagation of the probe may be neglected since $\left|\frac{dt}{t_0}\right| \gg \left|\frac{dL}{L_0}\right|$. Nonetheless, in materials with small elastic nonlinearity like polymers, metals, or non-bubbly fluids, this correction must be considered since $\left|\frac{dt}{t_0}\right|$ and $\left|\frac{dL}{L_0}\right|$ have the same order of magnitude.

13.3.3 *Investigating the Relation Between the Change of Wave-Speed of the Probe and the Magnitude of the Pump Stress/Strain*

We have explained how to obtain two time signals:

1. The change of travel time of the probe as a function of time (i.e., for each ultrasonic pulse of the sequence)
2. The pump strain experienced by the probe as a function of time (i.e., for each ultrasonic pulse of the sequence)

The magnitude of the change of travel time of the probe generally increases as the magnitude of the pump stress/strain is increased. Therefore, a typical experimental protocol includes repeating the measurement while varying the amplitude of the pump wave. Thus we generally have in hand a set of measurements performed with different pump amplitudes. At this point, one has two options to study the relation between the change of wave-speed of the probe and the magnitude of the pump stress/strain:

1. Plot the peak amplitude of the change of travel time of the probe as a function of the peak amplitude of the pump strain/stress
2. Plot the instantaneous change of travel time of the probe as a function of the instantaneous pump strain/stress.

For the first approach, the peak amplitude of the change of travel time of the probe can be estimated directly in the time domain or in the Fourier domain. If the repetition rate of the probe is more than twice larger than the frequency of the pump wave, then a fast Fourier transform can be computed and the amplitude of the variation evaluated. If the repetition rate of the probe is not sufficient to compute a fast Fourier transform (Nyquist criterion is not respected), then a Gram–Schmidt process can be used to decompose the signal, knowing the frequency of the pump wave [34]. Such an analysis is shown in Figs. 13.16, 13.17, and 13.18.

The second option is only possible if the recordings of the pump and the probe signals are properly synchronized. This is the method of choice if one is interested in details of the relation between the change of wave-speed of the probe and the magnitude of the pump stress/strain. Such an analysis is shown in Figs. 13.8, 13.9, 13.10, 13.11, 13.12, and 13.13 as well as Fig. 13.15.

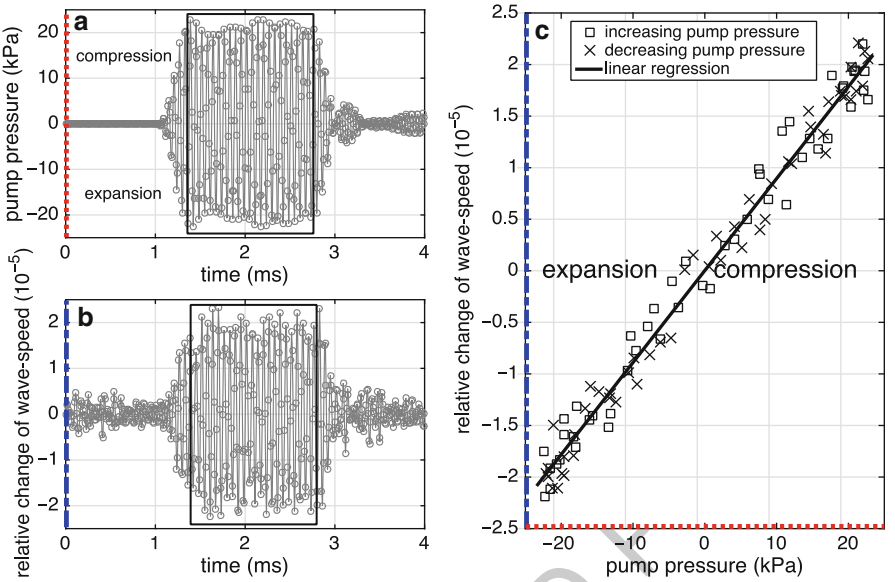

Fig. 13.8 Dynamic acousto-elastic response of water at 20 °C. The experimental setup shown in Fig. 13.5 was used. (**a**) Pump pressure as a function of time. (**b**) Relative change of speed of sound as a function of time obtained with the cross-correlation method. (**c**) Relative change of speed of sound as a function of the pump pressure. The two boxes in panels (**a**) and (**b**) show the data points that were selected to plot panel (**c**)

13.3.4 Alternative Measures of Acoustic Nonlinearity

Acoustic nonlinearity includes both elastic nonlinearity and dissipative nonlinearity. In our specific experimental situation, one investigates the effect of a "large-amplitude" pump wave on the propagation of a "small-amplitude" probe wave. The elastic nonlinearity of the material causes the acousto-elastic effect. In addition, in granular media or damaged/cracked media, the pump wave can also induce a variation in the attenuation experienced by the probe wave (dissipative nonlinearity).

The objective of a DAET measurement may be very practical, for instance, detecting and monitoring changes in a material like the accumulation of damage. In this case, the investigation of the change of wave-speed of the probe may not be the most sensitive parameter. The change of ultrasonic attenuation may be chosen as an alternative indicator of the level of damage [20, 37]. Such a change of ultrasonic attenuation can be simply implemented by tracking a change of the amplitude of the probe signal. Alternatively the cross-correlation method introduced earlier to estimate a change of travel time of the probe can be further exploited by tracking a change of the amplitude of the normalized cross-correlation function. If its amplitude equals 1 it means that the two input signals are identical waveforms (there may exist a time lag though). If the amplitude of the normalized cross-correlation function is less than 1, it means that the shape of the probe waveform has been modified, likely by a change of ultrasonic attenuation.

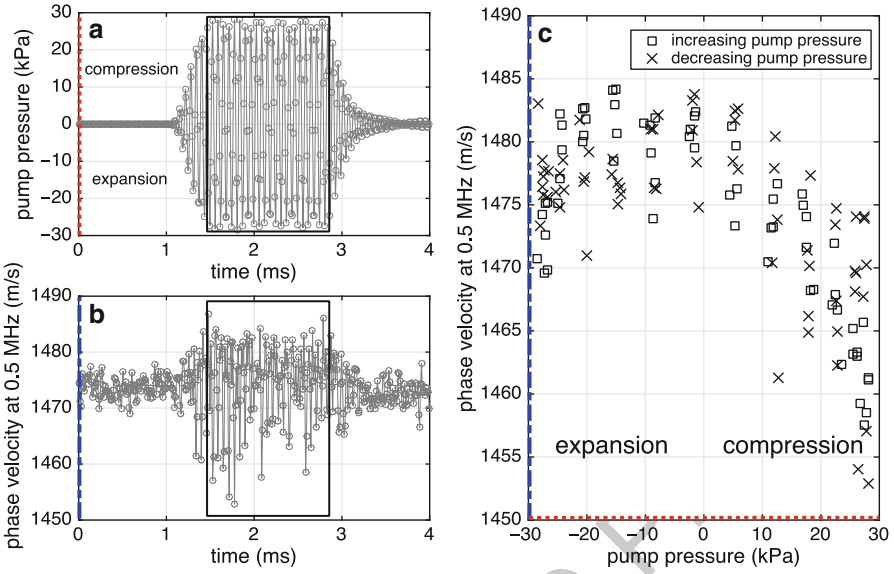

Fig. 13.9 Dynamic acousto-elastic response of a suspension of lipid-coated gas microbubbles in water at 0.5 MHz, i.e., at a frequency well below the resonance frequency of the microbubbles. The relative volume fraction occupied by microbubbles is 10^{-6}. The experimental setup shown in Fig. 13.5 was used. (**a**) Pump pressure as a function of time. (**b**) Phase velocity at 0.5 MHz as a function of time obtained with the frequency domain method. (**c**) Phase velocity at 0.5 MHz as a function of the pump pressure. The two boxes in panels (**a**) and (**b**) show the data points that were selected to plot panel (**c**)

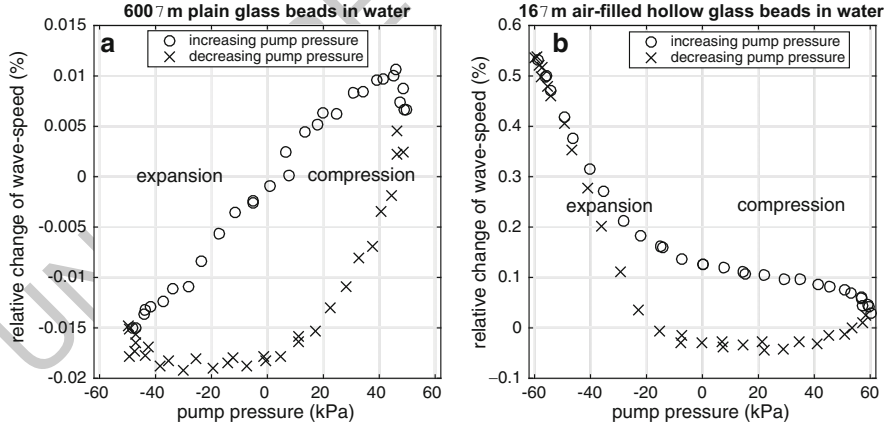

Fig. 13.10 Dynamic acousto-elastic response of (**a**) water-saturated plain glass beads with a diameter of 600 μm and (**b**) water-saturated air-filled hollow glass beads with a diameter of 16 μm. These measurements were performed with the system developed by RheaWave [25] which uses the experimental configuration described in Fig. 13.5

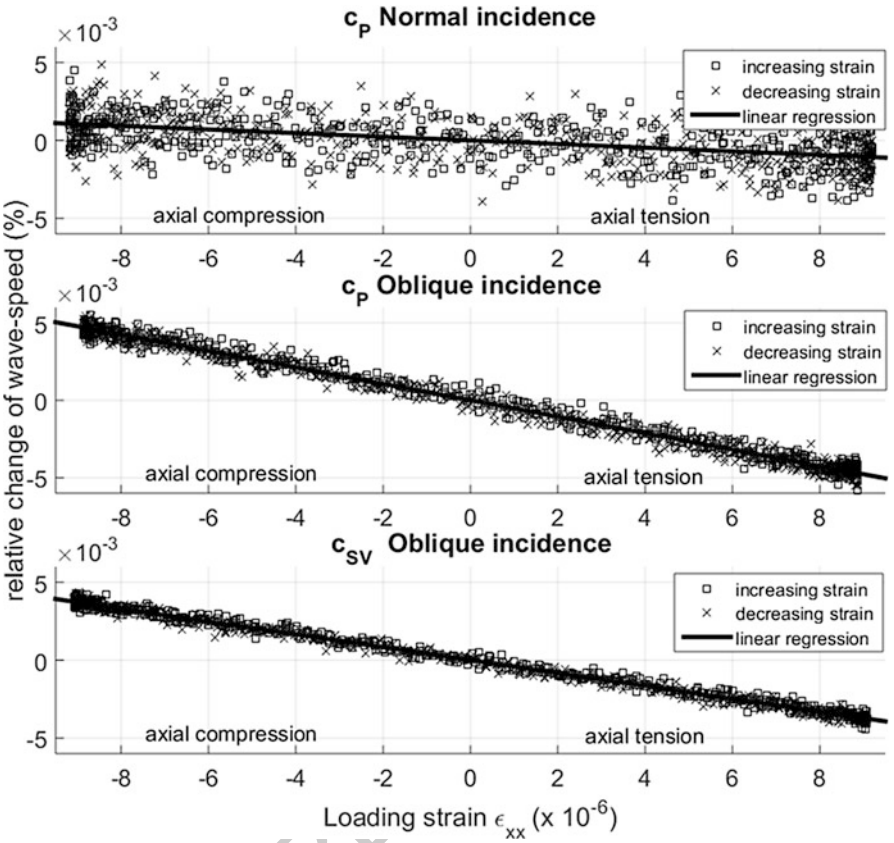

Fig. 13.11 Dynamic acousto-elastic response of PMMA with different orientations and types of US probe waves [41]. The orientations of the ultrasound transducers are chosen to probe the effect of a uniaxial strain (or stress) on the propagation velocity of compression bulk waves (c_P) with normal and oblique incidence and vertically polarized shear bulk waves (c_{SV}) with oblique incidence. The maximum axial strain is 9×10^{-6} while the relative change of wave-speeds varies between 0.001 and 0.005%

13.4 Observations in Different Materials

In this section, we present applications of dynamic acousto-elastic testing to different types of materials. This includes results in liquids and solids. We show how the addition of soft inclusions in a material, namely gas bubbles in a liquid or cracks in a solid, can dramatically change the dynamic acousto-elastic response of the material. More specifically, the reader shall appreciate that the addition of soft inclusions modifies the acousto-elastic effect quantitatively (soft inclusions enhance the elastic nonlinearity of the material) and qualitatively (hysteresis and DC component can appear).

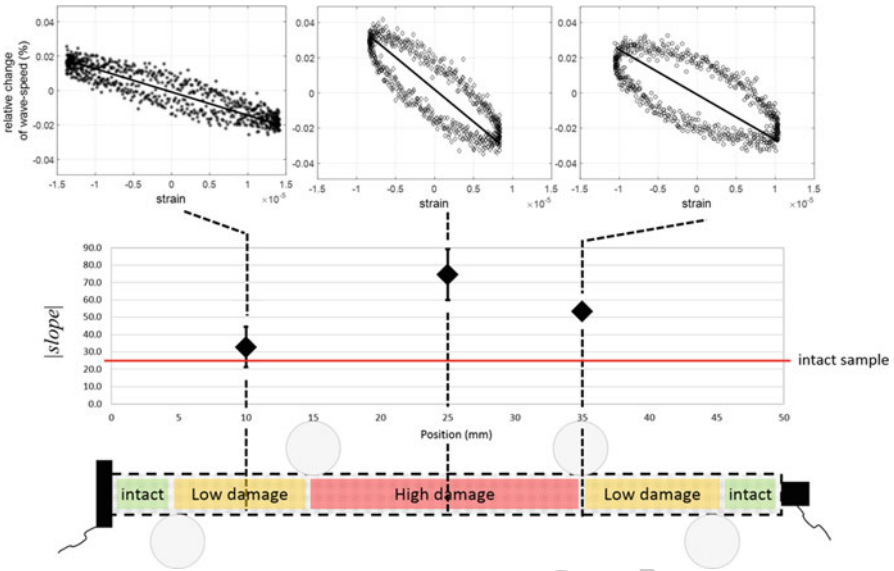

Fig. 13.12 Dynamic acousto-elastic responses measured at different positions along the fatigued bar of aluminum (i.e., 10, 25, and 35 mm). The slope and the hysteresis of the nonlinear signature are higher where the level of distributed fatigue damage is expected to be higher. Positive (negative) strain corresponds to tension (compression) phase of the sample

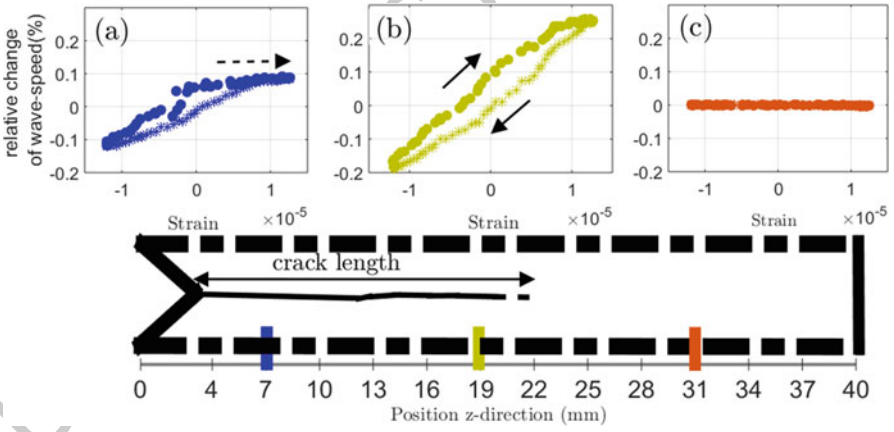

Fig. 13.13 Dynamic acousto-elastic responses for three characteristics positions along the sample width. Positive (negative) strain corresponds to tension (compression) phase of the sample

AQ4

13.4.1 Liquids

13.4.1.1 Non-Bubbly Liquid

A typical experimental setup to apply dynamic acousto-elastic testing in a fluid is depicted in Fig. 13.5. The pump wave is a 16 kHz pressure wave generated by an underwater acoustic projector. The probe wave is a short ultrasound burst with a center frequency of 4 MHz that is generated by an immersion broadband ultrasound transducer. The ultrasound transducer broadcasts a sequence of short ultrasonic pulses with a repetition rate of 100 kHz. A plastic block is used as a reflector placed in front of the ultrasound transducer so that the ultrasound transducer can be operated in pulse-echo mode to transmit and receive the probe wave. The amplitude of the pump wave is first measured by a hydrophone that is inserted between the ultrasound transducer and the reflector, i.e., on the path of the ultrasound pulse (while the probe is turned off). Then the actual experiment of dynamic acousto-elasticity is conducted by turning on both the probe wave and the pump wave. The broadcasting of the pump wave is delayed by 1 ms. This delay is useful to appreciate the level of noise in the measurement of the change of travel time of the probe wave. The state-of-the-art equipment typically provides a noise level of 0.1 nanosecond or less for the measurement of travel time changes of the probe wave (dt).

The change of travel time of the probe wave is calculated using the cross-correlation method. Figure 13.8a shows the pump pressure experienced by each probe pulse as a function of time and the panel b depicts the relative change of speed of sound in water $(c - c_0)/c_0$ as a function of time. Finally a plot of the relative change of speed of sound as a function of the pump pressure is shown in panel c. There are several points to highlight when analyzing panel c. Firstly the magnitude of the relative change of wave-speed is small; the change of travel time of the probe wave is close to 0.1 ns while the total travel time of the probe wave is 5.8 μs. Secondly panel c shows that the relation between the relative change of wave-speed and the pump pressure is linear, with no DC offset (the change of wave-speed is null at zero pump pressure) and no hysteresis. When the pump pressure is positive (medium compression) the wave-speed increases. Conversely, when the pump pressure is negative (medium expansion) the wave-speed decreases.

Finally it was shown that DAET allows one to estimate the parameter of nonlinearity B/A in fluids [19, 25]. The parameter of nonlinearity B/A is proportional to the slope coefficient of the linear relation observed in panel c of Fig. 13.8.

13.4.1.2 Liquid with Suspension of Gas MicroBubbles

The experimental setup depicted in Fig. 13.5 can be used to investigate the influence of the addition of micrometric particles in a fluid. Figure 13.9 shows the acousto-elastic response of a suspension of lipid-coated gas microbubbles in water. Those lipid-coated gas microbubbles are used as an ultrasound contrast agent for medical

ultrasonography. Even if the microbubbles occupy a relative volume fraction of only 10^{-6}, the acousto-elastic response of the suspension is dramatically changed compared to that of water only (Fig. 13.8). First the variation in wave-speed is two orders of magnitude larger. Secondly the compression of the medium imposed by the pump wave reduces the wave-speed, while an increase is observed in water only (Fig. 13.8). The suspension of microbubbles has a resonance frequency close to 2 MHz. For a frequency well below this resonance frequency, attenuation is very small and the wave-speed is determined by the compressibility of the mixture. Figure 13.9 shows the acousto-elastic response of the suspension at 0.5 MHz, it was obtained by applying a frequency domain analysis (see Sect. 13.3 of this chapter). At this frequency, the wave-speed is determined by the compressibility of the medium. The decrease of wave-speed during medium compression is likely caused by the reversible buckling of the lipid shell of the microbubbles [26]. When shell buckling occurs, the stiffness of medium suddenly collapses and the wave-speed decreases.

13.4.1.3 Water-Saturated Glass Beads

The acousto-elastic response of water-saturated plain glass beads was investigated [24, 25]. Figure 13.10 shows the results in water-saturated plain glass beads with a diameter of 600 μm and water-saturated air-filled hollow glass beads with a diameter of 16 μm. The probe signal was a short ultrasound burst with a center frequency of 0.6 MHz. The frequency of the pump wave was 3.7 kHz. The pump wave is expected to modulate the contacts between the glass beads. As a result complicated dynamic changes of the ultrasonic wave-speed are observed, including expansion-compression asymmetry, hysteresis, and DC offset.

13.4.2 Solids

13.4.2.1 Undamaged Homogeneous Solids

Dynamic acousto-elastic testing has been successfully applied to study the classical nonlinear elasticity of two isotropic materials—a polymer, the polymethyl methacrylate (PMMA) and an aluminum alloy [27, 41, 43]. In these studies, both PMMA and aluminum samples have a cylindrical shape; therefore, the LF pump wave is tuned to match the frequency (i.e., few kHz) of the first compressional mode (or first Pochhammer-Chree mode) as explained in Sect. 13.2.4. The LF pump wave is broadcasted directly in the sample by means of a piezoelectric disk glued on the sample. The vibration is measured by an accelerometer glued at the top of the sample. The experimental setup of the LF pump corresponds to the configuration shown in Figs. 13.2b and 13.4.

A sequence of ultrasonic short bursts (with a typical center frequency of 1 or 2 MHz) is simultaneously applied to measure the dynamic change of elasticity

induced by the pump wave. The experimental setup corresponds to the typical configuration shown in Fig. 13.3b but with different angles for the ultrasound transducers that transmit and receive the probe wave. The orientations of the ultrasound transducers are chosen to probe the effect of a uniaxial strain (or stress) on the propagation velocity of compressional bulk waves (c_P) with normal and oblique incidence and with vertically polarized shear bulk waves (c_{SV}) with oblique incidence. The maximal pump strain experienced by the US probe is close to 10^{-5}.

The changes in travel time of the probe wave (dt) for different strain levels are calculated using the cross-correlation method. Then, the TOF variation due to the Poisson effect is subtracted from the total TOF variation in order to retrieve the TOF variation solely due to the variation in wave-speed (Sect. 13.3).

The results are shown in Fig. 13.11. For undamaged homogeneous solids such as PMMA and aluminum, the relative variation of wave-speed is very weak (between 0.001 and 0.005%) and exhibits a linear relation with the pump strain. When the pump strain is negative (axial compression), the wave-speed increases. Conversely, when the pump strain is positive (axial tension), the wave-speed decreases. Neither a DC offset nor hysteresis is observed: the change of wave-speed is null when the pump strain is zero.

In particular, a larger variation of compression bulk wave-speed (c_P) is observed when the direction of propagation has an oblique incidence compared with normal incidence. Indeed, it is well established that, even though a homogeneous solid sample exhibits isotropic elastic properties, the effect of a uniaxial strain (or stress) induces wave-speed anisotropy [7]. The propagation velocity of an elastic wave depends on the angle between the propagation direction and the axis of the applied loading [8]. Therefore, the acousto-elastic effect is stronger when the propagation direction of the probe wave is parallel to the direction of the uniaxial loading (produced by the pump wave).

Finally, it has been shown that it is possible to estimate the three independent third-order elastic constants (TOEC) for isotropic materials with DAET, by combining three different carefully chosen configurations for the US probe [41].

13.4.2.2 Damaged Homogeneous Solids

In the past decades, several nonlinear acoustical techniques were proposed for in situ nondestructive testing (NDT), such as wave frequency mixing or resonance measurements. Among them, DAET provides a unique way to observe nonlinear elastic features over an entire dynamic stress cycle while other techniques measure average bulk variations of modulus versus strain level. DAET also provides a local measurement of the nonlinear elasticity, which is particularly convenient to localize and characterize microdamage within a whole solid.

It has been demonstrated that DAET applied to steel and aluminum samples is sensitive to

1. Distributed fatigue damage [32] and
2. A localized single micro-crack [31, 32].

The experimental setup involves a stationary pump wave and two compressional bulk wave transducers in transmission configuration as described in Fig. 13.4.

In case of the fatigue damage protocol [32], two aluminum bars (50 × 4 × 2 mm) are machined from the same 2 mm thick aluminum plate. The first aluminum specimen is fatigued while the second one is kept intact and serves as control. Fatigue damage is induced by cycling 10,000 times within the elastic regime using a four-point bending configuration. Dislocation density and/or fatigue cracking on the external surface is suspected to be larger in the center of the bar where the stress concentration is the maximum, while both ends of the bar remain intact. DAET measurements have been performed on both aluminum samples (i.e., intact and damaged) at different positions along the bar (i.e., 10, 25, and 35 mm). For each position, the relative change of wave-speed is plotted against strain level in Fig. 13.12. Then, the slope is extracted from each acousto-elastic response. Negative slopes are observed, as expected for most metals, with the highest value obtained in the center of the specimen, where fatigue damage is expected to be the most severe. Moreover, a hysteresis is present in the nonlinear signature. For the intact sample, no hysteresis is observable and the slopes (horizontal red line in Fig. 13.12) remain constant along the sample with an average value smaller than the slopes measured in the damage sample.

In case of the localized single micro-crack protocol [31], a closed fatigue crack has been formed in an aluminum alloy bar (170 × 30 × 40 mm) by a three-point bending fatigue test. The fatigue crack is extended from a notch placed at mid-length. The notch is approximately 3 mm deep and the fatigue crack is 17 mm long. The fatigue crack is invisible to the eye. Twelve DAET measurements have been performed along the crack (i.e., in the z-direction). Three typical acousto-elastic responses are shown in Fig. 13.13. No change in wave-speed is observed outside of the crack (Fig. 13.13c) whereas large changes are observed along the crack (Fig. 13.13a, b). The largest slope and hysteresis are observed close to the crack tip (Fig. 13.13b). At the notch, the crack is expected to be more open than at any other location. A bi-state behavior is clearly observed near the notch (Fig. 13.13a), with the presence of a plateau, i.e., no change in velocity during the tension phase when the crack is opened. Therefore, near the notch, the crack induces elastic nonlinearly essentially during the compression phase while elasticity is virtually unchanged in the tension phase. This agrees with a simple model of Contact Acoustic Nonlinearity [48, 49] that describes asymmetry between compression and tension phases. On the other hand, at the crack tip, the change of wave-speed is more symmetric and a high elastic nonlinearity (large slopes in Fig. 13.13b) is observed. Finally the positive sign of the slope is somewhat surprising as it means that the velocity decreases during the compression phase, which would imply that asperities at the interface slow down the direct wave. Further investigation will be needed to understand such behavior.

13.4.2.3 Rocks, Cementitious, and Granular Materials

Unlike undamaged or single-cracked materials, poorly consolidated media such as rocks and concrete exhibit very large nonlinear behaviors [50]. Perhaps the most striking feature is the appearance of a transient elastic softening, as soon as the medium is subjected to dynamic strains as low as 10^{-7} [27, 37]. It is then followed by a $\log(t)$ relaxation back to the original elastic modulus as soon as the dynamic loading is turned off [51]. This elastic softening is also often referred to as "conditioning," or "dynamically induced conditioning" or "DC offset." In some poorly consolidated media, the elastic modulus can therefore be transiently reduced by several percent, depending on the loading amplitude and frequency. Understanding such behavior is critical to better estimate seismic hazard, for instance, for civil structures and buildings. One key step towards the development of robust diagnostic tools is therefore to relate these complex nonlinear responses to physical, quantitative microstructural features.

Beyond nondestructive evaluation and civil engineering applications, there is growing evidence that such nonlinear effects are key mechanisms for the understanding of earthquake triggering, when a large seismic wave transiently softens the Earth's crust and triggers a second earthquake [52]. Current research also focuses on the link between elastic softening [53] and transient increases in permeability observed following earthquakes [54]. Such relation with fluid processes is of particular significance for the understanding of induced seismicity in oil/gas and geothermal applications.

As shown in Fig. 13.14, the sound speed evolution in highly nonlinear media such as rock, concrete, and granular media can be decomposed in six consecutive phases.

The initial phase (Phase I) refers to the beginning of the experiment when the pump is "off." In this phase, the unperturbed local wave-speed of the specimen is registered. Upon turning "on" the pump, the pump strain first rings up towards the steady state (Phase II). In Phase III, the pump strain has reached a steady state, but the sound speed continues to drop. Phase IV is the time domain where the medium is in a non-equilibrium steady state. By analyzing the strain-dependency of sound speed in this phase, the different nonlinear material properties can be evaluated, as discussed in the next section (Phase IV: During the Dynamic Loading). In Phase V, the pump strain rings down towards zero. Finally in Phase VI, the pump strain is zero, but the sound speed is still recovering. The slow recovery of sound speed towards the speed of sound at the initial unperturbed state is referred to as "slow dynamics" and will be further detailed in section "After the Dynamic Loading: Slow Dynamics (Phase VI)".

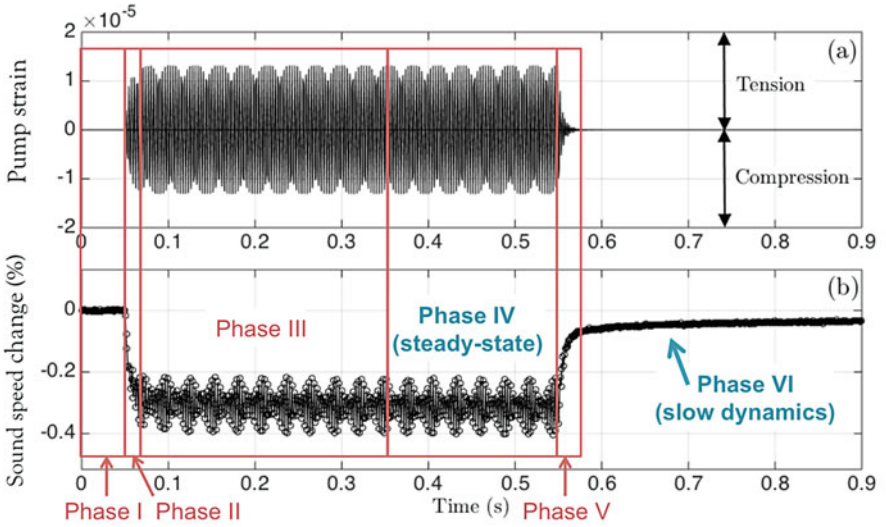

Fig. 13.14 Typical DAET results in a sample of Berea sandstone [28] using the experimental setup described in Fig. 13.4. The sound speed changes in response to the pump strain. The evolution of sound speed can be studied in six time domains (Phases I–VI). Details on the fast (Phase IV) and slow (Phase VI) dynamics responses are presented in sections "Phase IV: During the Dynamic Loading" and "After the Dynamic Loading: Slow Dynamics (Phase VI)," respectively

AQ5

Phase IV: During the Dynamic Loading

Instantaneous Velocity Changes

DAET is often performed at a single large strain amplitude, either to evaluate the third-order elastic constants in weakly nonlinear elastic materials (Fig. 13.11), to compare the nonlinear responses at different locations (Figs. 13.12 and 13.13), or to monitor a sample over time as it undergoes progressive damage. On the other hand, to further improve the theoretical description of nonlinear elasticity in complex (either damaged or granular-like) materials, one may want to perform DAET at multiple peak strain amplitudes, from a weakly nonlinear regime at low strain ($\sim 10^{-7}$) to a highly nonlinear regime at larger strain ($\sim 10^{-5}$).

Figure 13.15 shows some typical DAET results in two samples of Berea sandstone and Berkeley blue granite at room-dry conditions and multiple strain amplitudes ranging from 10^{-7} to 10^{-5}, using the experimental setup described in Fig. 13.4. Both samples exhibit a transient elastic softening that increases with the pump amplitude, reaching about $\sim 0.5\%$ at strain $\varepsilon_m = 8 \times 10^{-6}$. Further observations can be made depending on the strain range. At large strains ($\sim 10^{-5}$), complex loops are observed, with larger (lower) velocity during the compression (tension) phase, suggesting opening/closing of micro-cracks or grain contacts. This effect seems particularly strong for the granite sample (Fig. 13.15b). The acousto-elastic responses for the two samples differ at intermediate strains ($\sim 10^{-6}$); while

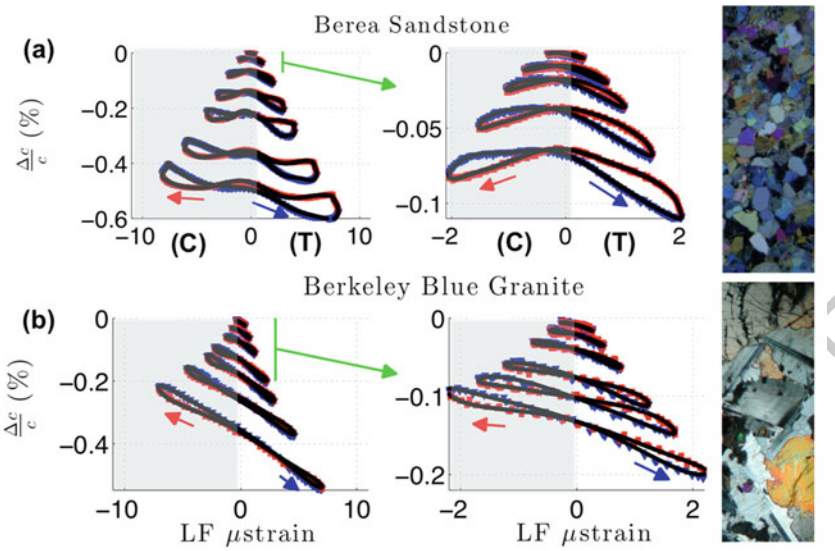

Fig. 13.15 Relative velocity change $\Delta c/c$ as a function of low-frequency pump strain ε for 10 increasing strain excitations ranging from 10^{-7} to 10^{-5}. (**a**) Berea sandstone. (**b**) Berkeley blue granite. Plots on the right side provide details on the nonlinear responses for strain amplitudes lower than 2×10^{-6}. Blue triangles (red squares) correspond to increasing (decreasing) strains. Negative strains correspond to the compression phase (C) whereas positive strains correspond to the tension phase (T). The black line shows the result of the Fourier analysis (cf. [28] for further details). On the right side, photomicrographs under plane polarized light. Height of the photo is 2.35 mm for Berea sandstone, 3.85 mm for Berkeley blue granite (Modified from [28])

the granite sample exhibits a larger velocity at negative pump strain (than at zero pump strain) and a smaller velocity at positive pump strain, the velocity in Berea sandstone at negative and positive pump strain maxima is found lower than at zero pump strain (right plots in Fig. 13.15). No certain evidence exists on a particular mechanism for such observation. However, the fact that it is observed for all tested sandstones [28, 43] suggests that it could arise from shearing processes at the grain boundaries, leading to a lower elastic modulus during maximum tension and compression, and larger moduli when strain passes through zero. Finally, the large slope for granite at intermediate and large strains suggests that the opening/closing mechanism dominates over shearing processes [43].

Amplitude Dependence

The dynamic acousto-elastic response of rocks is far more complicated than that of homogeneous undamaged solids (like PMMA, Fig. 13.11). While the velocity in homogeneous undamaged solids is modulated only at the frequency of the pump, the dynamic change of velocity in rocks exhibits a component at the frequency of the pump, at its higher harmonics as well as at zero frequency. To further investigate

the nonlinear elastic responses in rocks, the time series $\Delta c/c(t)$ can be decomposed using a Fourier analysis in combination with a Gram–Schmidt procedure [34]. The latter is needed to ensure orthogonality of the sine and cosine functions. From this analysis we find the amount of $\Delta c/c(t)$ oscillating at the pump frequency $\Delta c/c|_{\mathbf{1\omega}}$, twice the pump frequency $\Delta c/c|_{\mathbf{2\omega}}$, as well as the DC offset $\Delta c/c|_{\mathbf{0\omega}}$ (zero frequency component). When hysteretic effects are relatively small, as in Fig. 13.15, these quantities correspond approximately to the slope of the signature, the curvature, and the DC offset, respectively.

The $\Delta c/c|_{\mathbf{0\omega}}$—component is represented in Fig. 13.16 as a function of pump strain amplitude for both samples. This offset observed with DAET is equivalent to the frequency shift observed with NRUS (see Chap. 2 in this book) [28]. A progressive transition from quadratic dependence at low strain ($\sim 10^{-7}$) to linear at large strain ($\sim 10^{-5}$) is observed. This result, observed with both DAET [28, 34, 37] and NRUS [55], is typical of poorly cemented rocks. While no current theoretical model is able to fully capture the complex nonlinear response of rocks, cementitious, or granular-like materials, it is worth comparing these observations to some existing theories. One practical approach is to use the following 1D-equation (assuming material elastic nonlinearity is large and therefore neglecting changes in mass density):

$$\frac{\Delta M}{M} = 2\frac{\Delta c}{c} = \beta\varepsilon + \delta\varepsilon^2 + \alpha\left(\varepsilon_m + \text{sign}\left(\dot{\varepsilon}\right)\varepsilon\right),$$

where $\frac{\Delta M}{M}$, $\frac{\Delta c}{c}$, ε, $\dot{\varepsilon}$, and ε_m are, respectively, the relative change in modulus, the relative change in wave-speed, the pump strain, the strain rate, and the maximum strain excursion experienced by the material. The maximum strain excursion ε_m in our case is the amplitude of the pump strain, assuming $\varepsilon = \varepsilon_m \sin \omega t$. The terms β and δ represent the nonlinear quadratic and cubic coefficients, respectively, and arise from the classical nonlinear theory [7]. In particular, the term β is related to the third-order elastic coefficients (TOEC) [7]. The last term on the right-hand side results from the quadratic hysteretic nonlinear theory [50, 56–58]. Following such description, the quadratic dependence observed at low strain in Fig. 13.16 can be fitted with the cubic nonlinear parameter δ using $\left.\frac{\boldsymbol{\Delta M}}{M}\right|_{0\omega} = 2\left.\frac{\boldsymbol{\Delta c}}{c}\right|_{0\omega} = \frac{\delta\varepsilon_m^2}{2}$, whereas the linear dependence observed at large strain can be better fitted with the hysteretic parameter α using $\left.\frac{\boldsymbol{\Delta M}}{M}\right|_{0\omega} = 2\left.\frac{\boldsymbol{\Delta c}}{c}\right|_{0\omega} = \alpha\varepsilon_m$. However, it is important to note that such hysteretic model inherently couples hysteresis with softening which leads to an overestimation of hysteretic effects [34]. It also does not include the rate/frequency/relaxation effects that are described later.

Figure 13.17 shows the $\Delta c/c|_{\mathbf{1\omega}}$—component as a function of pump strain amplitude. The linear dependence over the whole strain range can be fitted with the classical quadratic nonlinear parameter β using $\left.\frac{\boldsymbol{\Delta M}}{M}\right|_{1\omega} = 2\left.\frac{\boldsymbol{\Delta c}}{c}\right|_{1\omega} = \beta\varepsilon_m$. The parameter β is found much larger in the granite sample than in the sandstone, as indicated by the larger slope observed for granite in Fig. 13.15.

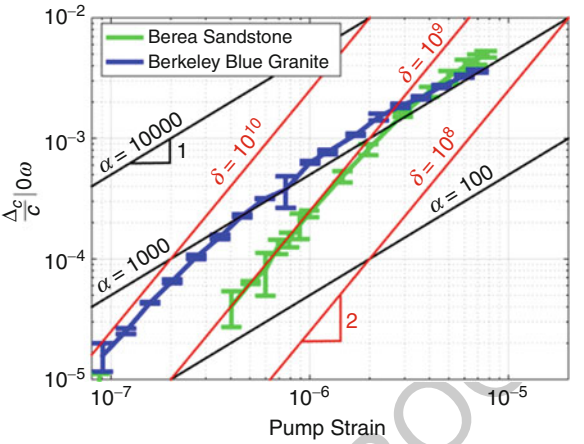

Fig. 13.16 Strain dependence for the offset component $\Delta c/c|_{0\omega}$ extracted from the Fourier analysis (black curves in Fig. 13.14) for two rock samples of Berea sandstone and Berkeley blue granite. This offset component corresponds to transient elastic softening that reaches about 0.5% at the maximum strain amplitude. Note the overall transition from quadratic to linear dependence as strain increases from 10^{-7} to 10^{-5}

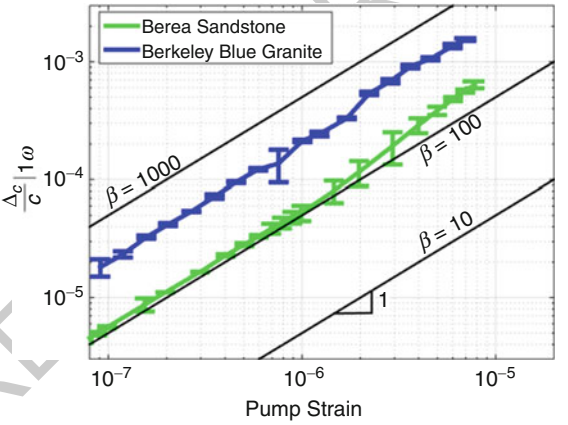

Fig. 13.17 Strain dependence for the slope component $\Delta c/c|_{1\omega}$ of Berea sandstone and Berkeley blue granite. Note the larger β value for the granite sample, as indicated by the larger slopes in Fig. 13.14

Figure 13.18 shows the $\Delta c/c|_{2\omega}$—component as a function of pump strain amplitude, related to the curvature shape in Fig. 13.15. As for the offset component, we observe a scaling change over the strain range considered [45]. It transitions from quadratic to roughly linear for the Berea sandstone, while the Berkeley blue granite is roughly linear at low strain and lower than 1 at large strain. The quadratic dependence at low strain for Berea can be fitted with δ using $\frac{\Delta M}{M}\Big|_{2\omega} = 2\,\frac{\Delta c}{c}\Big|_{2\omega} = \frac{\delta\varepsilon_m^2}{2}$. The parameter δ estimated from either the offset in Fig. 13.16 or the curvature in Fig. 13.18 leads to a value comprised between 10^8 and 10^9 for Berea sandstone (a larger value is found from the offset estimation).

The scaling changes observed for $\Delta c/c|_{0\omega}$ and $\Delta c/c|_{2\omega}$ occur at strains where higher order harmonics (in particular, $\Delta c/c|_{4\omega}$ and $\Delta c/c|_{6\omega}$) emerge from noise [28, 34]. Rather than using two models corresponding to two different strain ranges, an alternative approach consists in introducing a critical strain level ε_c at which the sample transitions from a quadratic to a linear dependence, using

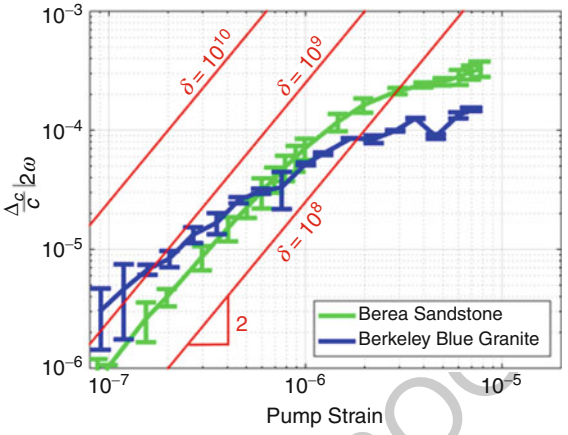

Fig. 13.18 Strain dependence for the curvature component $\boldsymbol{\Delta c/c|_{2\omega}}$ of Berea sandstone and Berkeley blue granite. As in Fig. 13.15 for the offset component, a progressive change in amplitude dependence is observed as strain increases from 10^{-7} to 10^{-5}

$\left.\frac{\Delta M}{M}\right|_{0\omega/2\omega} = 2\left.\frac{\Delta c}{c}\right|_{0\omega/2\omega} = \Gamma\varepsilon_c \tanh\frac{\varepsilon_m}{\varepsilon_c}\varepsilon_m$ (Guyer, personal note). This critical strain, a characteristic of the material, could then also be used to describe the emergence of higher order harmonics.

Finally, a third—more systematic—approach is used in [28] to compare the responses from 6 different rock samples. Ignoring the changes in scaling, each curve in Figs. 13.16, 13.17, and 13.18 is fitted over the whole strain range with $\left.\frac{\Delta c}{c}\right|_{n\omega} = a\varepsilon_m^{\nu}$. The power-law parameter ν is compared for all nonlinear components across samples. A correlation is found between the offset power-law $\nu_{0\omega}$, the curvature $\nu_{2\omega}$, and the hysteresis area of the loops ν_H, whereas the slope component $\nu_{1\omega}$ is found independent. This suggests that nonlinearity arises from two main mechanisms. The first one associated with the slope component $\Delta c/c|_{\mathbf{1\omega}}$ can be referred to as the classical nonlinearity, and as suggested above, is possibly related to opening/closing of cracks and grain contacts. The second one associated with all other components can be referred to as non-classical nonlinearity and is possibly related to shearing mechanisms of grain contacts.

Frequency Dependence: Transition from Static to Dynamic Acousto-Elasticity

One can ask whether the complex nonlinear effects measured at a few kilohertz still exist at much lower frequency. For instance, do these effects happen when a building vibrates at a few hertz due to the passage of seismic waves?

Both quasi-static tests and resonance-type experiments (see Chap. 2 in this book as well as [51, 59, 60]) have shown that rate effects are inherent to the nonlinear response of poorly cemented materials. For instance, when performing compressional tests on rocks, the hysteresis observed at typical experimental rate (~several minutes to an hour) can completely disappear if one performs the same test at a much lower rate (~several hours to a few days) [59]. This observation suggests that the system has enough time to recover from each incremental stress

step when cycled slowly: it remains in its original state and is not brought to a metastable state. On the other hand at larger rates, the initial increase in stress brings the sample to a new state and the subsequent decrease in stress does not follow the same path, leading to hysteresis. Resonance-type tests show similar behaviors when frequency is incrementally increased and decreased around the resonance frequency. The two upward and downward curves do not overlap when the test is performed quite fast, whereas they do overlap when the sweeps are conducted slowly [51]. To investigate such phenomena with DAET and provide further insights on the physical mechanisms at play, acousto-elastic measurements are performed at multiple loading frequencies ranging from quasi-static (~0.1 Hz) to dynamic (~10^3) regimes [61]. A rod-shaped sample of room-dry Berea sandstone is jacketed and placed upright in a pressure vessel. A large piezoelectric stack is forcing the sample to oscillate uniaxially. A small static overburden stress (0.5 MPa) is previously applied to maintain contact at all phases of the oscillation between the stack and the sample. Two longitudinal transducers operating at 500 kHz are glued on the sides of the sample to monitor the ultrasonic velocity before and during the steady-state oscillations. As for the standard DAET setup described in Fig. 13.4, the probing direction is normal to the loading direction. The Fourier analysis is performed on the nonlinear signatures and amplitudes $\Delta c/c|_{n\omega}$ are reported in Fig. 13.19 for frequencies spanning three orders of magnitude, constant strain amplitude ($\varepsilon = 1.4 \times 10^{-5}$), and constant confining pressure (1 MPa). Interestingly, the clustering found when studying multiple rocks at various strain amplitudes applies here too. Indeed, all nonlinear components but the slope ($\Delta c/c|_{1\omega}$) increase with frequency, suggesting that the mechanism related to $\Delta c/c|_{1\omega}$ is rather frequency independent (for instance, opening/closing of cracks). On the other hand, the frequency dependence observed for other components reinforces the assumption of friction/adhesion processes at crack interfaces and/or grain boundaries [62, 63].

The increase in nonlinearity with frequency corroborates former studies based on quasi-static and resonance tests [51, 59], that is, when dynamic tests are performed slowly enough, the specimen can continuously recover from the changes in loading conditions. Interestingly, the nonlinear components shown in Fig. 13.19 increase only by a factor 2 or 3 over 3 orders of magnitude in frequency, indicating that observations made at the laboratory scale in the kilohertz range are relevant to interpret larger scale observations (civil structures, geotechnical engineering, and seismology).

After the Dynamic Loading: Slow Dynamics (Phase VI)

The term “slow dynamics” was first used by [64] to describe the progressive recovery of the resonance frequency of rocks subsequent to acoustic straining or thermal shocking. Dynamic perturbations of sufficiently high amplitude (strain >10^{-6}) bring mesoscopic nonlinear materials such as rocks and cementitious materials [50] to a temporary metastable state that manifests itself by a sudden elastic softening (Phase II in Fig. 13.14). Once the perturbation is terminated, the elastic modulus slowly relaxes back towards its unperturbed equilibrium state (Phase VI in Fig. 13.14). This gradual transition of state is termed slow dynamics.

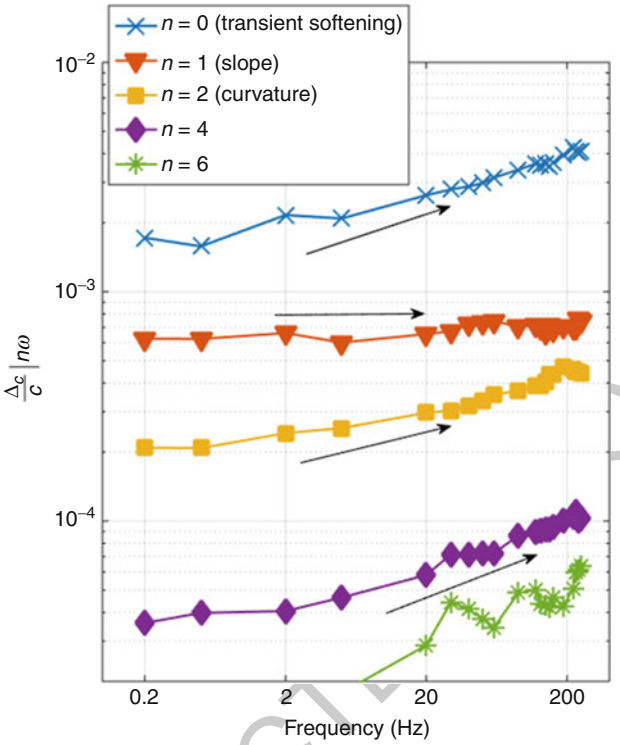

Fig. 13.19 Frequency dependence of the nonlinear components for a sample of Berea sandstone. All nonlinear components increase by a factor 2 or 3 over 3 orders of magnitude increase in frequency, except $\mathbf{\Delta c/c|_{1\omega}}$ (slope component) which is frequency independent. Note that these curves are obtained for a constant dynamic strain amplitude ($\varepsilon_m = 1.4 \times 10^{-5}$) and constant confining pressure (1 MPa). Similar observations are made at other confining pressures and oscillation amplitudes [61]

Early Time Vs. Late-Time Recovery

Earlier empirical observations have unanimously reported a time-logarithmic recovery at times t > 10 s after terminating the high-amplitude perturbation. The observed behavior appears to be independent of the test material or method used: resonance frequency in disparate rocks and concrete [64], Larsen frequency in cement paste and sandstone [65], and change of velocity in concrete [66]. Consequently, the handful of phenomenological models that have been developed to describe the post-perturbation recovery predict a log(t) behavior [67]. Despite the universal consensus about the time-logarithmic behavior, there is an experimental evidence for non-logarithmic recovery at earlier times, i.e., $t < 10$ s. For example, [65] have measured faster than log(t) relaxation in cement paste and sandstone at $t \sim 10^{-3}$. The recent model proposed by Snieder et al. [68] describes a multi-scale relaxation phenomenon that takes place on different temporal and spatial scales.

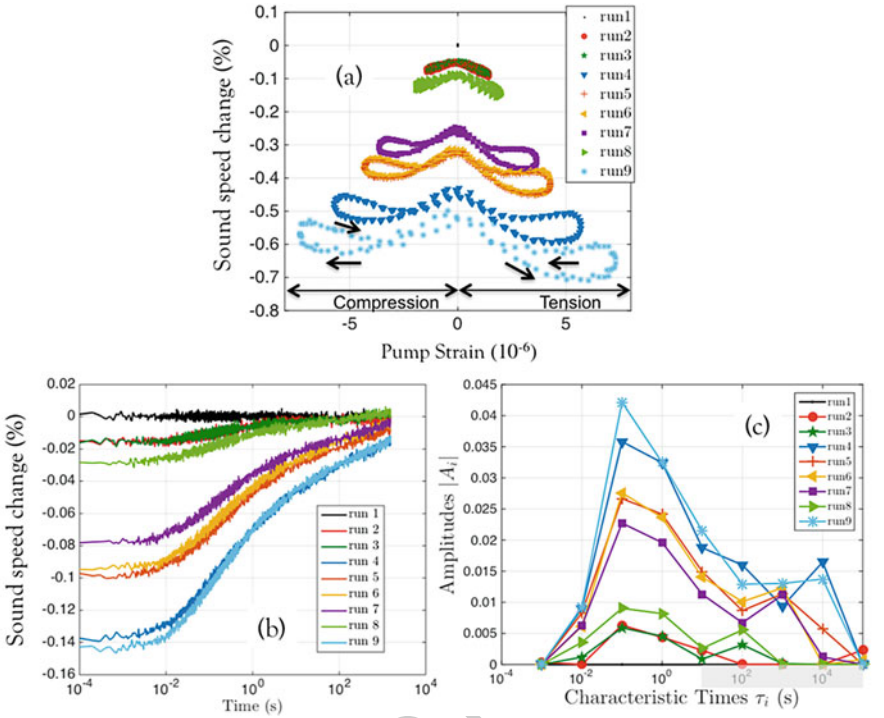

Fig. 13.20 DAET results on a sample of Berea sandstone. Runs 1–9 correspond to different pump strains: (**a**) Relative change in sound speed vs. pump strain during the non-equilibrium steady-state phase (Phase IV); (**b**) Progressive recovery of sound speed in Phase VI; (**c**) The corresponding relaxation spectra show a non-logarithmic recovery behavior at early times ($t < 10$ s). At later times, the spectrum is rather flat; the recovery is time-logarithmic, as found in previous studies [64]

DAET provides an unprecedented opportunity to investigate the recovery of mesoscopic nonlinear materials at times as early as $t \sim 10^{-4}$ s. Here, we present the results from a series of DAET experiments on a sample of Berea sandstone (Shokouhi et al. in preparation, to appear in 2017). The test apparatus, configuration, and parameters are very similar to those presented in [28] except that the sound speed is probed for a much longer time (about 30 min) after stopping the pump. Further, the test is conducted under controlled temperature $T(°C) = 23.0 \pm 0.2$ and relative humidity $RH(\%) = 50.0 \pm 0.2$ conditions. Figure 13.20 presents the obtained results; the sound speed variations with pump strain at steady state (Fig. 13.20a) and the corresponding recoveries (Fig. 13.20b).

An examination of the recovery behavior suggests that the material recovers faster at $t > 10^{-2}$ s than at later times $t > 10$ s, after which the recovery appears to progress time-logarithmically. For a more quantitative representation, the observed recoveries are described in the form of an exponential series $\sum_{i=1}^{9} A_i e^{-t/\tau_i}$, where relaxation times τ_i are equally distributed (in a logarithmic way) over the entire

time range. We find that a summation of nine exponentials is sufficient to fit the data without over fitting. The contribution of each exponential term to the recovery (A_i) or the "recovery spectrum" is shown in Fig. 13.20c. The recovery spectrum is a plot of exponential amplitudes A_i vs. the corresponding relaxation times τ_i.If wave-speeds were recovering time-logarithmically (i.e., linearly with $\log_{10}(t)$), the spectrum would be flat as was previously observed with resonance-based studies [64]. Unlike these studies, where later time recoveries were probed ($\tau \geq 10$ s), the early time recovery ($\tau < 10$ s) demonstrates preferential recovery time characteristics; the dominant recovery time for the sample is in the order of 10^{-1} s. Interestingly, the relaxation spectra for ($\tau \geq 10$ s) are almost flat, in close agreement with the earlier observations. Finally, the level of pump strain does not seem to alter the overall shape of the relaxation spectra; they all show a dominant recovery time at about 10^{-1} s. This latter observation suggests a link between the preferential recovery time and the rock microstructure. In fact, our recent observations indicate that the shape of the recovery spectrum is invariant to the changes in relative humidity of the test medium. While increasing the relative humidity increases the nonlinearity, it does not affect the multi-scale recovery rates. This latter observation provides additional evidence for the association of the recovery and microstructure. Furthermore, damage-induced microstructural changes have shown to alter the materials slow dynamics behavior. Earlier studies have shown that damage slows down the late-time recovery of cementitious materials. For example, TenCate et al. [64] show that damaged concrete recovers much slower than intact concrete. Tremblay et al. [66] made similar observations when comparing the late-time recoveries of an intact vs. a stress-damaged concrete sample. The study by Kodjo et al. [69] suggests that the rate of recovery may be used to differentiate two damage processes in concrete.

AQ6

We use DAET to investigate the influence of damage on early and late-time recoveries (Shokouhi et al., Ultrasonics, 2017, in press). Figure 13.21 compares the recoveries for two concrete samples: one intact and the other one damaged. Damage is induced by compressing one specimen to about 70% of its strength. The two specimens are from the same concrete mixture and visually indistinguishable (no visible surface cracking). Ultrasonic wave velocities measured (using compressional wave transducers of center frequency of 150 kHz) at two different locations across the samples are very similar. The damaged specimen has even a slightly higher linear dynamic modulus than the intact one: $E_{\text{intact}} = 33.1$ GPa and $E_{\text{damaged}} = 33.3$ GPa. Those moduli are measured by resonance ultrasonic spectroscopy (RUS) testing in the kHz range [70]. Despite their similar linear acoustic properties, the two samples differ significantly in terms of nonlinear signatures (Fig. 13.21a). The relaxation spectra in Fig. 13.21c show that the substantial recovery of the intact sample takes place for $t < 1$ s, whereas the damaged sample is still recovering even after 1 s. This observation suggests that damage-induced microstructural changes alter both fast and slow dynamics behaviors and that both signatures can be used to infer the state of damage in materials.

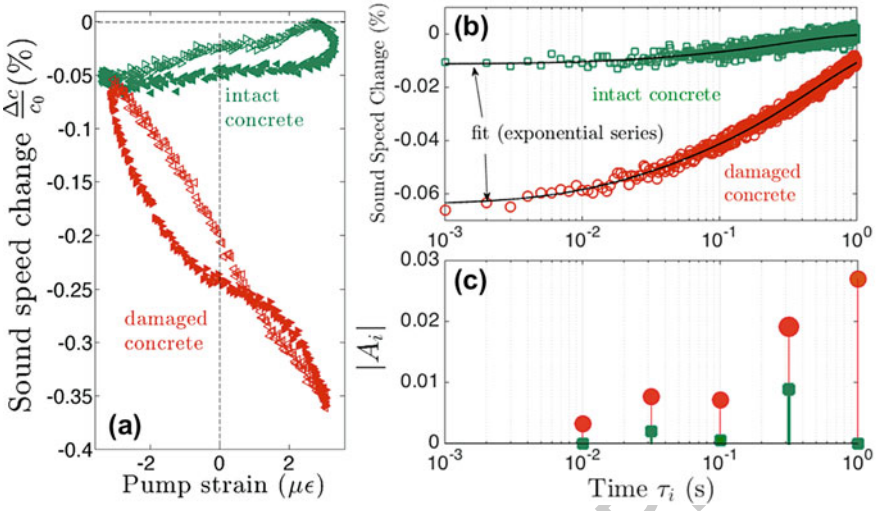

Fig. 13.21 Influence of damage on the DAET response of two concrete samples. (**a**) Fast dynamics response of intact and damaged concrete samples (phase IV). (**b**) Slow dynamics response (phase VI). (**c**) Corresponding relaxation spectra. Less than a second is needed for the intact sample to recover, whereas the damaged sample continues to recover after 1 s

13.5 Conclusions

The objective of Dynamic Acousto-Elastic Testing (DAET) is the measurement of the dynamic stress (or strain) dependence of the elasticity of a material at the micro-strain level. In a typical DAET experiment, two elastic waves are simultaneously generated in a material, a low-frequency pump wave and a sequence of identical high-frequency probe waves. The sequence of probe waves determines the local changes of wave-speed induced by the pump wave. These changes can be related to local changes of elasticity of the material. Unlike methods like nonlinear resonant ultrasound spectroscopy and nonlinear wave mixing, DAET reveals the details of the nonlinear elastic behavior over a single wave cycle, including hysteresis and expansion-compression asymmetry. While non-bubbly fluids or homogeneous undamaged solids exhibit a weak and simple dynamic acousto-elastic response, bubbly liquids and damaged or granular solids show large and complicated dynamic acousto-elastic responses. Thus DAET can be a useful technique for nondestructive evaluation of materials.

References

1. P.W. Bridgman, Water, in the liquid and five solid forms, under pressure. Proc. Am. Acad. Arts Sci. **47**, 441–558 (1912)
2. F. Birch, The effect of pressure on the modulus of rigidity of several metals and glasses. J. Appl. Phys. **8**, 129–133 (1937)
3. P. Van't Klooster, N.J. Trappeniers, S.N. Biswas, Effect of pressure on the elastic constants of noble metals from -196 to $+25^{\circ}$C and up to 2500 bar. Physica B **97**(1), 65–75 (1979)
4. J.C. Swanson, Pressure coefficients of acoustic velocity for nine organic liquids. J. Chem. Phys. **2**, 689–693 (1934)
5. J.R. Pellam, J.K. Galt, Ultrasonic propagation in liquids: I. Application of pulse technique to velocity and absorption measurements at 15 Megacycles. J. Chem. Phys. **14**(10), 608–614 (1946)
6. D. Lazarus, The variation of the adiabatic elastic constants of KCl, NaCl, CuZn, Cu, and Al with pressure to 10,000 Bars. Phys. Rev. **76**(4), 545–553 (1949)
7. A.N. Norris, *Nonlinear Acoustics* (Academic, New York, 1998), pp. 263–277
8. D.S. Hughes, J.L. Kelly, Second-order elastic deformation of solids. Phys. Rev. **92**(5), 1145–1149 (1953)
9. T. Bateman, W.P. Mason, H.J. McSkimin, Third-order elastic moduli of germanium. J. Appl. Phys. **32**(5), 928–936 (1961)
10. P.B. Nagy, Fatigue damage assessment by nonlinear materials characterization. Ultrasonics **36**, 375–381 (1998)
11. J.R. Asay, D.L. Lamberson, A.H. Guenther, Pressure and temperature dependence of the acoustic velocities in polymethylmethacrylate. J. Appl. Phys. **40**(4), 1768–1783 (1969)
12. K.W. Winkler, L. McGowan, Nonlinear acoustoelastic constants of dry and saturated rocks. J. Geophys. Res. **109**, B10204 (2004)
13. S. Haussühl, W. Chmielewski, Third-order elastic constants of orthorhombic calcium formate. Acta Crystallogr. Sect. A **37**(3), 361–364 (1981)
14. J.K. Krüger, C. Grammes, K. Stockem, R. Zietz, M. Dettenmaier, Nonlinear elastic properties of solid polymers as revealed by Brillouin spectroscopy. Colloid Polym. Sci. **269**(8), 764–771 (1991)
15. G. Gremaud, M. Bujard, W. Benoit, The coupling technique: a two-wave acoustic method for the study of dislocation dynamics. J. Appl. Phys. **61**(5), 1795–1805 (1987)
16. X. Jacob, C. Christophe Barriere, D. Royer, Acoustic nonlinearity parameter measurements in solids using the collinear mixing of elastic waves. Appl. Phys. Lett. **82**(6), 886–888 (2003)
17. A. Zeiger, K. Jassby, Measurement of acoustoelastic coefficients of Rayleigh waves in steel alloys. J. Nondestruct. Eval. **3**(2), 115–124 (1982)
18. R. Ellwood, T. Stratoudaki, S.D. Sharples, M. Clark, M.G. Somekh, Determination of the acoustoelastic coefficient for surface acoustic waves using dynamic acoustoelastography: an alternative to static strain. J. Acoust. Soc. Am. **135**(3), 1064–1070 (2014)
19. G. Renaud, S. Callé, J.-P. Remenieras, M. Defontaine, Exploration of trabecular bone nonlinear elasticity using time-of-flight modulation. IEEE Trans. UFFC **55**(7), 1497–1507 (2008)
20. G. Renaud, S. Callé, M. Defontaine, Remote dynamic acoustoelastic testing: elastic and dissipative acoustic nonlinearities measured under hydrostatic tension and compression. Appl. Phys. Lett. **94**, 11905 (2009)
21. P.J. Westervelt, Scattering of sound by sound. J. Acoust. Soc. Am. **29**(2), 199–203 (1957)
22. L.H. Taylor, F.R.J. Rollins, Ultrasonic study of three-phonon interactions. I. Theory. Phys. Rev. **136**(3A), A59–A596 (1964)
23. H. Moreschi, S. Callé, S. Guerard, D. Mitton, G. Renaud, M. Defontaine, Monitoring trabecular bone microdamage using a dynamic acousto-elastic testing method. Proc. Inst. Mech. Eng. **225**(3), 282–295 (2010)
24. G. Renaud, M. Defontaine, S. Callé, Dynamic acoustoelastic testing of weakly pre-loaded unconsolidated water-saturated glass beads. J. Acoust. Soc. Am. **128**(6), 1–11 (2010)

25. C. Trarieux, S. Callé, H. Moreschi, G. Renaud, M. Defontaine, Modeling nonlinear viscoelasticity in dynamic acoustoelasticity. Appl. Phys. Lett. **105**(26), 264103 (2014)
26. G. Renaud, J.G. Bosch, A.F. van der Steen, N. de Jong, Dynamic acousto-elastic testing applied to a highly dispersive medium and evidence of shell buckling of lipid-coated gas microbubbles. J. Acoust. Soc. Am. **138**(5), 2668–2677 (2015)
27. G. Renaud, M. Talmant, S. Callé, M. Defontaine, P. Laugier, Nonlinear elastodynamics in micro-inhomogeneous solids observed by head-wave based dynamic acoustoelastic testing. J. Acoust. Soc. Am. **130**(6), 3583–3589 (2011)
28. J. Rivière, P. Shokouhi, R.A. Guyer, P.A. Johnson, A set of measures for the systematic classification of the nonlinear elastic behavior of disparate rocks. J. Geophys. Res. Solid Earth **120**(3), 1587–1604 (2015)
29. D. Bui, S.A. Kodjo, P. Rivard, B. Fournier, Evaluation of concrete distributed cracks by ultrasonic travel time shift under an external mechanical perturbation: study of indirect and semi-direct transmission configurations. J. Nondestruct. Eval. **32**(1), 25–36 (2013)
30. Q.A. Vu, V. Garnier, J.F. Chaix, C. Payan, M. Lott, J.N. Eiras, Concrete cover characterisation using dynamic acousto-elastic testing and Rayleigh waves. Constr. Build. Mater. **114**, 87–97 (2016)
31. J. Rivière et al., Dynamic acousto-elasticity in a fatigue-cracked sample. J. Nondestruct. Eval. **33**(2), 216–225 (2014)
32. S. Haupert, J. Rivière, B. Anderson, Y. Ohara, T.J. Ulrich, P. Johnson, Optimized dynamic acousto-elasticity applied to fatigue damage and stress corrosion cracking. J. Nondestruct. Eval. **33**(2), 226–238 (2014)
33. M. Scalerandi, A.S. Gliozzi, S. Haupert, G. Renaud, M. Ait Ouarabi, F. Boubenider, Investigation of the validity of dynamic acoustoelastic testing for measuring nonlinear elasticity. J. Appl. Phys. **118**(12), 124905 (2015)
34. J. Rivière, G. Renaud, R.A. Guyer, P.A. Johnson, Pump and probe waves in dynamic acousto-elasticity: comprehensive description and comparison with nonlinear elastic theories. J. Appl. Phys. **114**(5), 54905 (2013)
35. T. Gallot, A. Malcolm, T.L. Szabo, S. Brown, D. Burns, M. Fehler, Characterizing the nonlinear interaction of S- and P-waves in a rock sample. J. Appl. Phys. **117**(3), 34902 (2015)
36. M. Lott et al., Three-dimensional treatment of nonequilibrium dynamics and higher order elasticity. Appl. Phys. Lett. **108**(14), 141907 (2016)
37. G. Renaud, J. Rivière, S. Haupert, P. Laugier, Anisotropy of dynamic acoustoelasticity in limestone, influence of conditioning, and comparison with nonlinear resonance spectroscopy. J. Acoust. Soc. Am. **133**(6), 3706–3718 (2013)
38. J.N. Eiras, Q.A. Vu, M. Lott, J. Payá, V. Garnier, C. Payan, Dynamic acousto-elastic test using continuous probe wave and transient vibration to investigate material nonlinearity. Ultrasonics **69**, 29–37 (2016)
39. B. Hilloulin et al., Monitoring of autogenous crack healing in cementitious materials by the nonlinear modulation of ultrasonic coda waves, 3D microscopy and X-ray microtomography. Constr. Build. Mater. **123**, 143–152 (2016)
40. M.A. Ouarabi, F. Boubenider, A.S. Gliozzi, M. Scalerandi, Nonlinear coda wave analysis of hysteretic elastic behavior in strongly scattering media. Phys. Rev. B **94**(13), 134103 (2016)
41. G. Renaud, M. Talmant, G. Marrelec, Microstrain-level measurement of third-order elastic constants applying dynamic acousto-elastic testing. J. Appl. Phys. **120**(13), 135102 (2016)
42. M. Lott, M.C. Remillieux, P.-Y. Le Bas, T.J. Ulrich, V. Garnier, C. Payan, From local to global measurements of nonclassical nonlinear elastic effects in geomaterials. J. Acoust. Soc. Am. **140**(3), EL231–EL235 (2016)
43. G. Renaud, P.-Y. Le Bas, P.A. Johnson, Revealing highly complex elastic nonlinear (anelastic) behavior of Earth materials applying a new probe: dynamic acoustoelastic testing. J. Geophys. Res. **117**(B6), B06202 (2012)
44. C. Payan, T.J. Ulrich, P.-Y. Le Bas, T. Saleh, M. Guimaraes, Quantitative linear and nonlinear resonance inspection techniques and analysis for material characterization: Application to concrete thermal damage. J. Acoust. Soc. Am. **136**(2), 537–546 (2014)

45. G. Renaud et al., In situ characterization of shallow elastic nonlinear parameters with dynamic acoustoelastic testing. J. Geophys. Res. Solid Earth **119**(9), 6907–6923 (2014)
46. J.A. TenCate, A.E. Malcolm, X. Feng, M.C. Fehler, The effect of crack orientation on the nonlinear interaction of a P wave with an S wave. Geophys. Res. Lett. **43**(12), 6146–6152 (2016)
47. I. Céspedes, Y. Huang, J. Ophir, S. Spratt, Methods for estimation of subsample time delays of digitized echo signals. Ultrason. Imaging **17**, 142–171 (1995)
48. I.Y. Solodov, N. Krohn, G. Busse, CAN: an example of nonclassical acoustic nonlinearity in solids. Ultrasonics **40**(1–8), 621–625 (2002)
49. S. Delrue, K. Van Den Abeele, Three-dimensional finite element simulation of closed delaminations in composite materials. Ultrasonics **52**(2), 315–324 (2012)
50. R.A. Guyer, P.A. Johnson, *Nonlinear Mesoscopic Elasticity* (Wiley, New York, 2009)
51. J.A. TenCate, Slow dynamics of earth materials: an experimental overview. Pure Appl. Geophys. **168**(12), 2211–2219 (2011)
52. P.A. Johnson, X. Jia, Nonlinear dynamics, granular media and dynamic earthquake triggering. Nat. Lett. **437**(6), 871–874 (2005)
53. F. Brenguier, M. Campillo, C. Hadziioannou, N.M. Shapiro, R.M. Nadeau, E. Larose, Postseismic relaxation along the san andreas fault at parkfield from continuous seismological observations. Science **321**(5895), 1478–1481 (2008)
54. J.E. Elkhoury, E.E. Brodsky, D.C. Agnew, Seismic waves increase permeability. Nature **441**(7097), 1135–1138 (2006)
55. D. Pasqualini, K. Heitmann, J.A. TenCate, S. Habib, D. Higdon, P.A. Johnson, Nonequilibrium and nonlinear dynamics in Berea and Fontainebleau sandstones: low-strain regime. J. Geophys. Res. **112**, B01204 (2007)
56. K.R. McCall, Theoretical study of nonlinear elastic wave propagation. J. Geophys. Res. Solid Earth **99**(B2), 2591–2600 (1994)
57. K.E.-A. Van Den Abeele, P.A. Johnson, A. Sutin, Nonlinear elastic wave spectroscopy (NEWS) techniques to discern material damage, part I: nonlinear wave modulation spectroscopy (NWMS). Res. Nondestruct. Eval. **12**, 17–30 (2000)
58. K.R. McCall, R.A. Guyer, Equation of state and wave propagation in hysteretic nonlinear elastic materials. J. Geophys. Res. **99**(12), 23,887–23,897 (1994)
59. K.E. Claytor, J.R. Koby, J.A. TenCate, Limitations of Preisach theory: elastic aftereffect, congruence, and end point memory. Geophys. Res. Lett. **36**(6), L06304 (2009)
60. J.A. TenCate, T.J. Shankland, Slow dynamics in the nonlinear elastic response of Berea sandstone. Geophys. Res. Lett. **23**(21), 3019–3022 (1996)
61. J. Rivière et al., Frequency, pressure, and strain dependence of nonlinear elasticity in Berea sandstone. Geophys. Res. Lett. **43**, 2016GL068061 (2016)
62. V. Gusev, V. Tournat, Amplitude- and frequency-dependent nonlinearities in the presence of thermally-induced transitions in the Preisach model of acoustic hysteresis. Phys. Rev. B **72**, 054104 (2005)
63. C. Pecorari, A constitutive relationship for mechanical hysteresis of sandstone materials. Proc. R. Soc. Lond. Math. Phys. Eng. Sci. **471**(2184), 20150369 (2015)
64. J.A. TenCate, E. Smith, R.A. Guyer, Universal slow dynamics in granular solids. Phys. Rev. Lett. **85**(5), 1020–1023 (2000)
65. O.I. Lobkis, R.L. Weaver, On the Larsen effect to monitor small fast changes in materials. J. Acoust. Soc. Am. **125**(4), 1894–1905 (2009)
66. N. Tremblay, E. Larose, V. Rossetto, Probing slow dynamics of consolidated granular multicomposite materials by diffuse acoustic wave spectroscopy. J. Acoust. Soc. Am. **127**(3), 1239–1243 (2010)
67. O.O. Vakhnenko, V.O. Vakhnenko, T.J. Shankland, J.A. Ten Cate, Strain-induced kinetics of intergrain defects as the mechanism of slow dynamics in the nonlinear resonant response of humid sandstone bars. Phys. Rev. E **70**(1), 015602 (2004)
68. R. Snieder, C. Sens-Schönfelder, R. Wu, The time dependence of rock healing as a universal relaxation process, a tutorial. Geophys. J. Int. **208**(1), 1–9 (2017)

69. A.S. Kodjo, P. Rivard, F. Cohen-Tenoudji, J.-L. Gallias, Impact of the alkali–silica reaction products on slow dynamics behavior of concrete. Cem. Concr. Res. **41**(4), 422–428 (2011)
70. T.J. Ulrich, K.R. McCall, R.A. Guyer, Determination of elastic moduli of rock samples using resonant ultrasound spectroscopy. J. Acoust. Soc. Am. **111**(4), 1667–1674 (2002)